Electronic Supplementary Information

Donor-acceptor complex formation by social self-sorting of polycyclic aromatic hydrocarbons and perylene bisimides

Simon Soldner,[a] Olga Anhalt,[a] Menyhárt B. Sárosi,[a,b] Matthias Stolte,[a,b] Frank Würthner[a,b]*

[a] Center for Nanosystems Chemistry (CNC), Universität Würzburg, Theodor-Boveri-Weg, 97074 Würzburg, Germany

[b] Institut für Organische Chemie, Universität Würzburg, Am Hubland, 97074 Würzburg, Germany

*E-mail: wuerthner@uni-wuerzburg.de

Table of Contents

1. Materials and methods

All chemicals, reagents and solvents were purchased from commercial suppliers and used after appropriate purification if not stated otherwise. All reactions were done under inert conditions. The PBIs and the belonging amines were synthesized according to literature known procedures.[S1-S5] Toluene used for synthesis was of HPLC grade and was dried prior to use utilizing a *Pure Solv MD 7* system from *Inert Technology*. Dichloromethane (DCM) was distilled prior to use. Dry tetrahydrofuran (THF) was used for synthesis. Column chromatography was performed using commercial glass columns packed with silica gel 60 M (particle size of 0.04 - 0.063 mm from Merck KGaA) stationary phase. Normal phase HPLC was performed on a *JASCO* recycling semipreparative HPLC system equipped with a VP 250/21 NUCLEOSIL 100-7 column from *Macherey-Nagel*.

UV/Vis spectroscopy was carried out at room temperature on a *JASCO V770* spectrophotometer. Solution spectra were taken using 0.1, 1, 10 and 100 mm cuvettes (SUPRASIL®, Hellma® Analytics) and solvents dichloromethane, chloroform, methylcyclohexane (MCH) and 1,1,2,2-tetrachloroethane (TCE) were of spectroscopic grade. For concentration-dependent UV/Vis studies, stock solutions were stepwise diluted before each measurement.

Fluorescence spectroscopy was carried out on a *FLS98-D2D2-ST0* fluorescence spectrometer from *Edinburgh Instruments*. Spectra were corrected against the photomultiplier sensitivity and the lamp intensity. Fluorescence quantum yields (Φ_f) were determined using the relative method and *N,N'*-Bis(2,6-diisopropylphenyl)-perylene-3,4:9,10-bis(dicarboximide) with Φ_f = 100% as reference.[S6] Fluorescence lifetimes were determined with EPL picosecond pulsed diode lasers (λ_{ex} = 505.8 nm) for time correlated single photon counting.

NMR spectroscopy was performed using Bruker *Avance III HD* 400 and 600 MHz NMR spectrometers. Chemical shifts (δ) are listed in parts per million (ppm) relative to residual undeuterated solvent signals. The multiplicities for proton signals are abbreviated as d, t, quin, sep. and m for doublet, triplet, quintet, septet and multiplet, respectively.

Solution-state complexation studies. UV/Vis absorption and fluorescence titration experiments were conducted by applying the constant-host routine in chloroform, methylcyclohexane and tetrachloroethane solution. For this purpose, a solution of host (c_0(**3a**, **3b**, **3c**) = 10^{-5} - 10^{-7} M) with a defined excess of guest was titrated to a pure host solution with the same PBI concentration. The obtained data were fitted globally with a 1:1 and 1:2 binding model by a nonlinear regression method using the program bindfit[S7] from Thordarson and colleagues.[S8]

High resolution mass: MALDI-TOF measurements were performed on a *Bruker Daltonics* ultrafleXtreme mass spectrometer. Trans-2-[3-(4-*tert*-butylphenyl)-2-methyl-2-propenylidene]-malononitrile (DCTB) was used as the matrix. ESI-TOF was performed on the *micoTOF focus* instrument from *Bruker Daltonics*.

Melting points were determined using a SMP50 from *Stuart Equipment*.

Single crystal X-ray diffraction. Measurements were performed at 100 K on *Bruker's D8 Quest Kappa diffractometer* with a *Photon II CPAD* as detector. The diffraction data were processed with the help of the APEX3 and APEX4 program packages. The structure was solved with the help of the SHELXT[S9] software and subsequently further processed using Fourier techniques, where SHELX[S10] software was used. The PLATON SQUEEZE program was used to remove the contributions of disordered solvent molecules.[S11- S12] Crystallographic data are deposited on the Cambridge Crystallographic Data Centre as supplementary publication numbers CCDC2284853 (**3a**), CCDC2284854 (**3b**), CCDC2284855 [P·**3a**·P] and CCDC2284856 [T·**3a**·T].

(Photoluminescence) polarization microscopy and spectroscopy of single crystals. (Photoluminescence) Polarization microscopy images of micrometre-sized single crystals on quartz substrates were recorded with a *Zeiss Axio Imager optical polarization microscope*. (Polarization-dependent) Localized absorption spectra of individual single crystals were measured with the same microscope with a customized spot resolution down to 1 x 1 µm^2 (A. S. & Co GmbH) coupled to an *Ocean Optics Maya 2000Pro® spectrometer* and referenced against the transmission of the neat quartz substrate. Localized fluorescence spectra of individual single crystals were also measured with the same setup under blue light excitation (464 - 495 nm) and corrected for the dark noise of the spectrometer.

Computational methods. The conformation of the dimers in solution might differ from the orientation adopted in the crystal structures. To generate the dimer conformations, the monomers were docked into each other with xtb 6.6.0[S13] at the GFN2-xTB level.[S14] The obtained dimer structures were further optimized with ORCA 5.0.4[S15] at the r^2-SCAN-3c level.[S16] Since the alkyl-phenyl arms are expected to play negligible or no role in the exciton coupling between the two PBI units, they were replaced with H atoms in the optimized dimer structures of both **3a** and **3b**. These newly added hydrogen atoms were geometry optimized relative to the fixed remaining atomic positions at the r^2-SCAN-3c level. The Coulomb (J_{Coul}) and charge-transfer (J_{CT}) couplings were calculated according to a protocol successfully applied for characterising PBI folda-dimers.[S17] The overall coupling (J) is the sum of J_{Coul} and J_{CT}. In contrast to the previously published protocol, J_{Coul} was computed based on transition charges from electrostatic potential (TrESP)[S18] and using MultiWFN.[S19] The data necessary for J_{Coul} was obtained from ωB97X-D/def2-SVP TD-DFT calculations using Gaussian 16.[S20] The hole/electron transfer integrals (t_h and t_e, respectively) were calculated with ADF2013.[S21] The level of theory in ADF2013 was chosen and J_{CT} was computed according to our published protocol.[S16] Starting from the crystal structure coordinates, the geometries of both P·**3a**·P and T·**3a**·T complexes were optimized at the r^{2}SCAN-3c level, and subsequently their excited states were calculated with ωB97X-D/def2-SVP. Both sets of calculations employed the CPCM(chloroform) solvent model. Similar calculations were carried out for the **3b** monomer. Natural transition orbitals (NTOs) were calculated with MultiWFN.[S18] The optimized geometries were also used for the energy decomposition analyses (EDA) based on the absolutely localized molecular orbital (ALMO) approach.[S22] ALMO-EDA results were obtained from D3(zero)-B3LYP/6-311G* single point calculations in Q-Chem 5.1.2.[S23] Molecular structures and orbitals were rendered with UCSF Chimera.[S24]

2. Synthesis

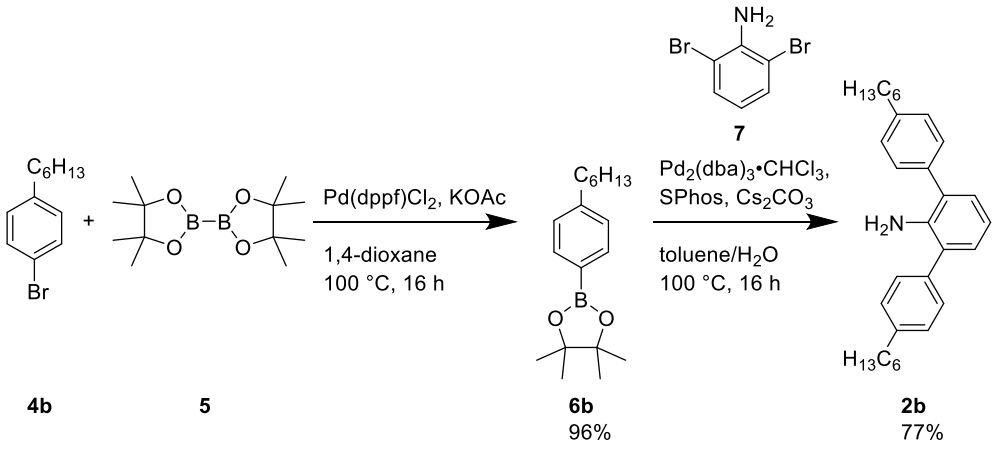

Scheme S1. Synthesis of the amine **2b**.

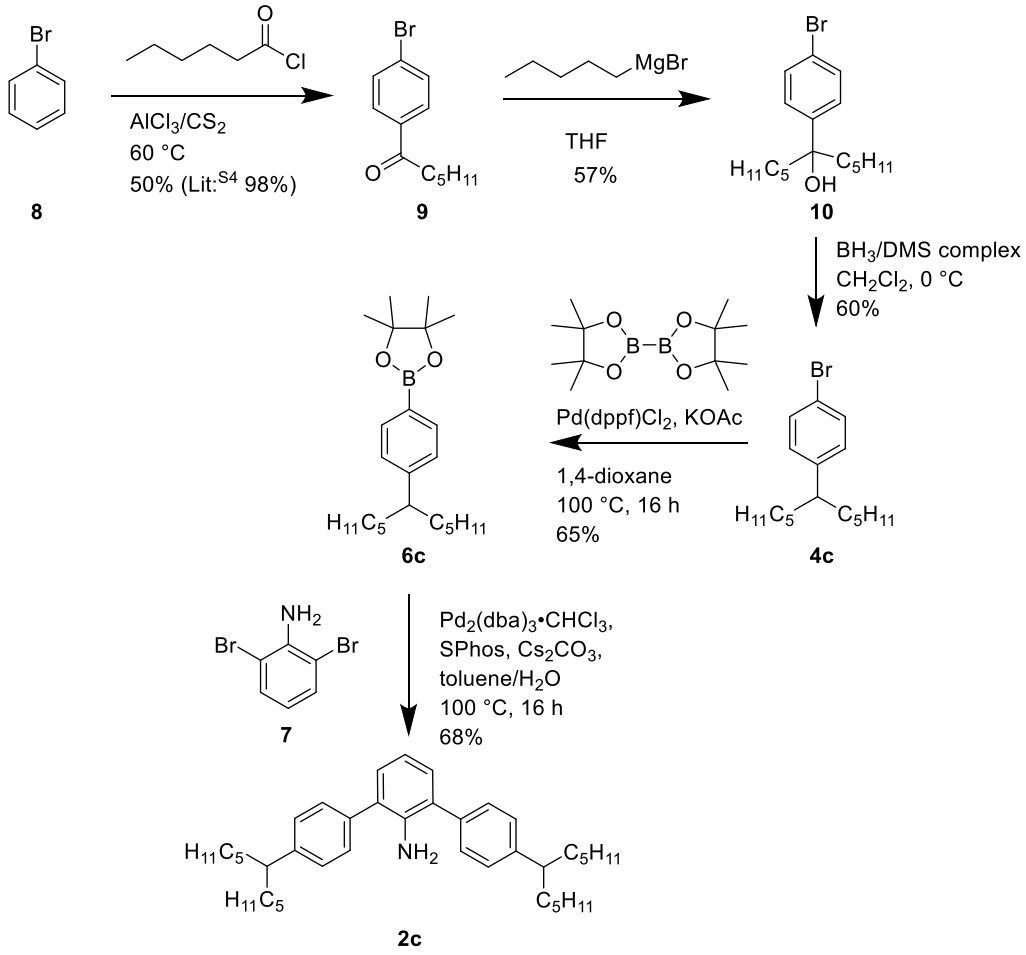

Scheme S2. Synthesis of the amine **2c**.

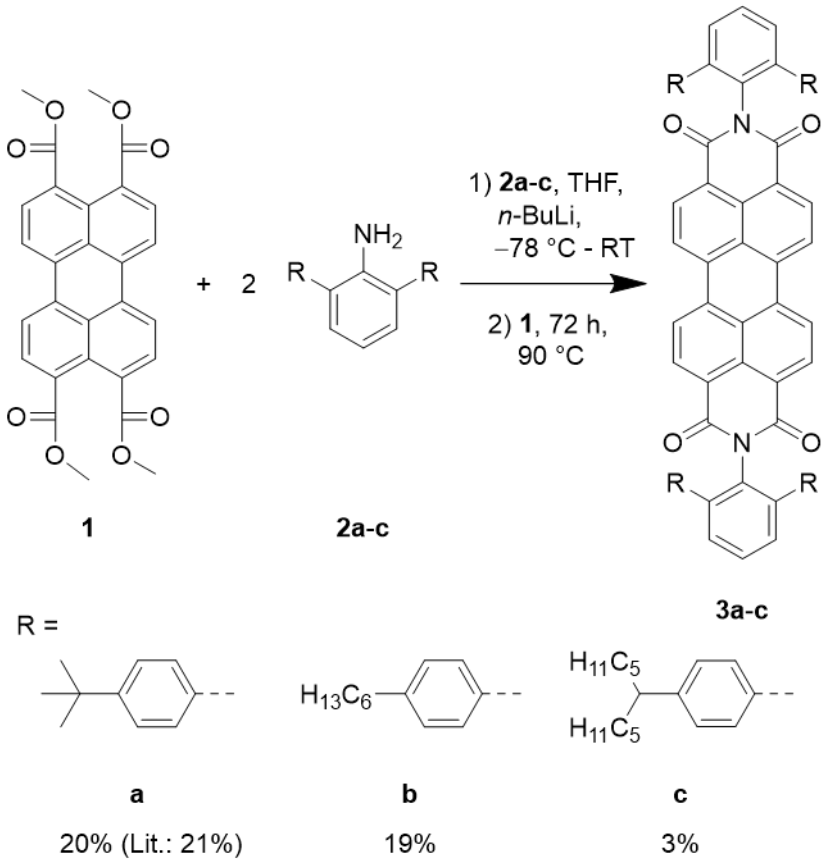

Scheme S3. Synthesis of the PBIs **3a**-**c**. **3a** was synthesized as described in literature.[S1]

Synthesis of 1-(4-Bromophenyl)-1-hexanone (**9**):

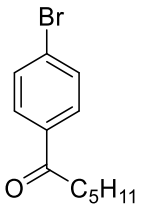

9

Under a nitrogen atmosphere, hexanoyl chloride (9.78 mL, 70.4 mmol, 1.0 eq.) was dissolved in dry carbon disulphide (100 mL) and cooled to 0 °C. The solution was stirred and aluminum trichloride (13.3 g, 100 mmol, 1.4 eq.) was added. After 15 minutes, bromobenzene (7.37 mL, 70.4 mmol, 1.0 eq.) dissolved in dry carbon disulphide (50 mL) was added dropwise from a dropping funnel over 20 minutes, while the temperature was maintained at 0 °C. Then, the mixture was heated at 60 °C for 10 h. Afterwards, a solution of 10% aq. HCl was added to the mixture. The organic layer was extracted with dichloromethane, washed with brine, dried over $MgSO_4$ and concentrated under vacuum. The crude product was recrystallized in dichloromethane and methanol. All data are the same as described in the literature.[S4]

Yield: 8.93 g (35.0 mmol, 50%) of a white solid.

Synthesis of α,α-dipentyl-4-bromobenzyl alcohol(10):

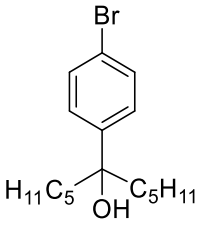

10

At first, the Grignard-reagent was synthesized under nitrogen atmosphere according to literature.[S25] Magnesium (2.61 g, 108 mmol, 2.5 eq.) was baked out three times. Then, two iodine spheres were added and sublimated. THF (48 mL) and 1-pentylbromide (5.33 mL, 43.0 mmol, 1.0 eq.) were added. The mixture was stirred for 1 h at 50 °C. 1-(4-Bromophenyl)-1-hexanone (4.50 g, 17.6 mmol, 1.0 eq.) was dissolved in THF (29 mL) and the Grignard-reagent (6.19 g, 35.3 mmol, 2.0 eq.) was added and the mixture was stirred at 50 °C for 12 h. After cooling down to room temperature, a dilute aqueous solution of NH_4Cl (50 mL) was given into the mixture. After extraction with dichloromethane, washing with brine, drying over $MgSO_4$ and removal of the solvent the crude product was purified by column chromatography (dichloromethane/cyclohexane = 1/4).

Yield: 3.29 g (10.1 mmol, 57%) of a yellow oil.

^{1}H-NMR (400 MHz, $CDCl_3$, 298 K): δ/ppm = 7.44 (d, *J* = 8.89 Hz, 2H), 7.25 (d, *J* = 8.89 Hz, 2H), 1.82-1.72 (m, 4H), 1.31-1.15 (m, 12 H), 0.84 (t, *J* = 7.22 Hz, 12H).

^{13}C-NMR (101 MHz, $CDCl_3$, 298 K): δ/ppm = 145.7, 131.2, 127.3, 120.2, 77.0, 43.1, 32.3, 23.2, 22.6, 14.1.

Synthesis of 1-Bromo-4-(1-pentylhexyl)-benzene (**4c**):

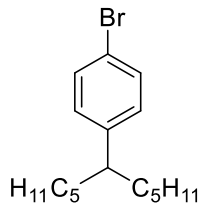

4c

The alcohol (**10**) (4.08 g, 12.5 mmol, 1.0 eq.) was dissolved in dry dichloromethane (89 mL) and cooled to −5 °C under nitrogen atmosphere. Methanesulfonic acid (1.8 mL) was added. After 30 minutes borane-dimethyl sulphide complex solution (1.0 M in dichloromethane) (25.0 mL, 25.0 mmol, 2.0 eq.) was added. The mixture was stirred for another 2 h at this temperature. The reaction was treated with addition of a $NaHCO_3$ solution (5%). The organic layer was extracted with dichloromethane, dried over $MgSO_4$ and concentrated under vacuum. The crude product was purified by column chromatography (cyclohexane).

Yield: 2.33 g (7.47 mmol, 60%) of a yellow oil.

^{1}H-NMR (400 MHz, $CDCl_3$, 298 K): δ/ppm = 7.41 (d, *J* = 9.63 Hz, 2H), 7.03 (d, *J* = 10.08 Hz, 2H), 2.45 (sep., *J* = 4.58 Hz, 1H), 1.64-1.46 (m, 4 H), 1.27-1.11 (m, 12H), 0.84 (t, *J* = 7.50 Hz, 6H).

^{13}C NMR (101 MHz, $CDCl_3$, 298 K): δ/ppm = 145.5, 131.4, 129.6, 119.4, 45.7, 37.0, 32.0, 27.3, 22.7, 14.2.

Synthesis of 2-(4-Hexylphenyl)-4,4,5,5-tetramethyl-1,3,2-dioxaborolane (6b):

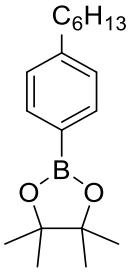

7b

1-Bromo-4-hexylbenzene (5.00 g, 20.7 mmol, 1.0 eq.), bis(pinacolato)diborone (6.84 g, 27.0 mmol, 1.3 eq.), potassium acetate (6.96 g, 70.9 mmol, 3.4 eq.), and Pd(dppf)Cl_2 (303 mg, 0.41 mmol, 2%) were dissolved in degassed 1,4-dioxane (25 mL). The mixture was stirred at 100 °C for 16 h. After cooling to room temperature, saturated ammonium chloride solution (50 mL) and water (75 mL) were added to the reaction mixture. Extraction was carried out with diethyl ether (75 mL three times each). The combined organic phases were washed with water (50 mL) and saturated NaCl solution (50 mL) and dried over magnesium sulfate. The solvent was removed under reduced pressure. The crude product was purified by column chromatography (silica, dichloromethane/cyclohexane = 1/1). The data are in agreement with the literature.[S3]

Yield: 5.73 g (19.9 mmol, 96 %) of a yellowish oil.

^{1}H-NMR (400 MHz, $CDCl_3$, 298 K): δ/ppm = 7.72 (d, *J* = 8.0 Hz, 2H), 7.19 (d, *J* = 7.9 Hz, 2H), 2.54, (t, *J* = 15.5 Hz, 2H), 1.65-1.58 (m, 2H), 1.33 (s, 12H), 1.32-1.25 (m, 6H), 0.87 (t, *J* = 13.9 Hz, 3H).

Synthesis of 2-(4-(1-pentylhexyl)phenyl)-4,4,5,5-tetramethyl-1,3,2-dioxaborolane (6c):

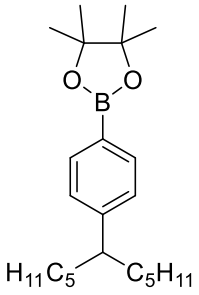

7c

Under vacuum **6** (4.45 g, 14.3 mmol, 1.0 eq.), bis(pinacolato)diboron (4.72 g, 18.6 mmol, 1.3 eq.), KOAc (4.80 g, 48.9 mmol, 3.4 eq.) and Pd(dppf)Cl_2 (209 mg, 290 µmol, 2%) were dissolved in degassed dioxane (17 mL). The mixture was heated up to 100 °C for 16 h. Saturated NH_4Cl (50 mL) and water (75 mL) were added after cooling to room temperature. The organic phase was extracted with diethyl ether (3 × 75 mL), dried over $MgSO_4$ and concentrated under vacuum. The crude product was purified by column chromatography (dichloromethane/cyclohexane = 1/1).

Yield: 3.30 g (9.21 mmol, 65%) of a greenish oil.

^{1}H-NMR (400 MHz, $CDCl_3$, 298 K): *δ*/ppm = 7.75 (d, *J* = 7.70 Hz, 2H), 7.17 (d, *J* = 7.70 Hz, 2H), 2.49 (sep., *J* = 5.57 Hz, 1H), 1.62-1.49 (m, 4H,), 1.34 (s, 12H), 1.25-1.11 (m, 12H), 0.82 (t, *J* = 6.93 Hz, 6H).

^{13}C-NMR (101 MHz, $CDCl_3$, 298 K): *δ*/ppm = 150.1, 134.9, 127.3, 83.7, 46.4, 37.0, 32.1, 27.4, 25.0, 22.7, 14.2.

MS (MALDI-TOF, pos. Mode, DCM): *m/z* calcd. for $C_{23}H_{39}BO_2Na$: 381.29408; found 381.29312 $[M+Na]^+$.

Synthesis of 2,6-Bis(4-hexylphenyl)aniline (2b):

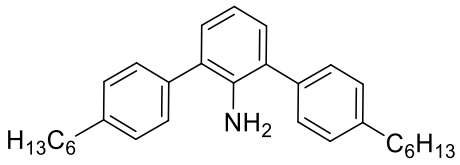

2b

2,6-Dibromaniline (88.4 mg, 352 µmol, 1.0 eq.), 2-(4-hexylphenyl)-4,4,5,5-tetramethyl-1,3,2-dioxaborolane (**7b**) (234 g, 810 µmol, 2.3 eq.), caesium carbonate (344 g, 1.06 mmol, 3.0 eq.), $Pd_2(dba)_3{\cdot}CHCl_3$ (18.2 mg, 17.6 µmol, 5%) and SPhos (28.9 mg, 70.5 µmol, 20%) were dissolved in dry degassed tetrahydrofuran (26 mL) and water (13 mL). The mixture was stirred at 100 °C for 16 hours. After cooling to room temperature, the mixture was extracted with dichloromethane, washed with water, and dried over magnesium sulfate. The solvent was removed under reduced pressure. The crude product was purified by column chromatography (silica, from dichloromethane/cyclohexane = 1/9 to 3/7). The data are in agreement with the literature.[S3]

Yield: 112 mg (271 µmol, 77%) of a yellow oil.

^{1}H-NMR (400 MHz, CD_2Cl_2, 298 K): δ/ppm = 7.52 (d, *J* = 7.86 Hz, 4 H), 7.36 (d, *J* = 8.32 Hz, 4 H), 7.21 (d, *J* = 6.94 Hz, 2 H), 6.95 (t, *J* = 8.32 Hz, 1 H), 3.95 (s, 2 H), 2.76 (t, *J* = 6.98 Hz, 4 H), 1.77 (quin, *J* = 7.00 Hz, 4 H), 1.51-1.39 (m, 12 H), 1.02 (t, *J* = 5.58 Hz, 6 H).

Synthesis of 2,6-Bis(4-(1-pentylhexyl)phenyl)aniline (2c):

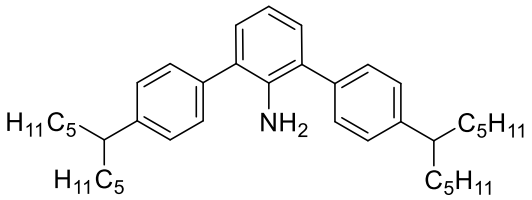

2c

2,6-Dibromoaniline (1.00 g, 3.99 mmol, 1.0 eq.), **7c** (3.28 g, 9.17 mmol, 2.3 eq.), caesium carbonate (3.90 g, 12.0 mmol, 3.0 eq.) $Pd_2(dba)_3{\cdot}CHCl_3$ (207 mg, 200 µmol, 5%) and SPhos (328 mg, 800 µmol, 20%) were dissolved in degassed toluene (13 mL) and water (6.5 mL) under nitrogen atmosphere. The mixture was heated at 100 °C for 16 h. The organic layer was extracted with dichloromethane, dried over $MgSO_4$ and concentrated under vacuum. The crude product was purified by column chromatography (dichloromethane/cyclohexane = 1/9).

Yield: 1.51 g (2.73 mmol, 68%) of a yellow oil.

^{1}H-NMR (400 MHz, $CDCl_3$, 298 K): δ/ppm = 7.45 (d, *J* = 7.66 Hz, 4H), 7.25 (d, *J* = 7.66 Hz, 4H), 7.16 (d, *J* = 7.66 Hz, 2H), 6.89 (t, *J* = 8.62 Hz, 1H), 3.93 (s, 2H), 2.59-2.51 (m, 2H), 1.72-1.55 (m, 8H), 1.32-1.18 (m, 24H), 0.90-0.86 (m, 12H).

^{13}C-NMR (101 MHz, $CDCl_3$, 298 K): δ/ppm = 145.6, 141.1, 137.2, 129.6, 129.1, 128.2, 118.1, 45.9, 37.0, 32.1, 27.5, 22.7, 14.2.

MS (MALDI-TOF, pos. Mode, DCM): *m/z* calcd. for $C_{40}H_{59}N$: 553.46475; found: 553.46600.

Synthesis of 3,4,9,10-Perylenetetracarboxylic acid tetramethyl ester (1):

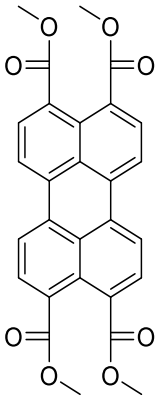

1

3,4,9,10-Perylenetetracarboxylic acid dianhydride (2.00 g, 5.10 mmol, 1.0 eq.) was suspended in methanol (25 mL) and acetonitrile (50 mL). Methyl iodide (3.17 mL, 7.24 g, 51.0 mmol, 10 eq.) was dropped to the reaction mixture. At 0 °C, 1,8-diazabicyclo[5.4.0]undec-7-ene (6.09 mL, 6.21 g, 40.8 mmol, 8.0 eq.) was added. The mixture was then heated at 65 °C for 6 days. After cooling, a 10% ammonia solution (25 mL) was added. Dichloromethane was used for extraction and the combined organic phases were washed with water and dried over magnesium sulfate. The solvent was removed under reduced pressure and the residue was recrystallized in dichloromethane/methanol. The data are in agreement with the literature.[S1]

Yield: 1.81 g (3.74 mmol, 73%) of an orange solid.

^{1}H-NMR (400 MHz, $CDCl_3$, 298 K): δ/ppm = 8.37 (d, J = 8.05 Hz, 4 H), 8.09 (d, J = 8.05 Hz, 4 H), 3.94 (s, 12 H).

Synthesis of *N,N`*-Bis[2,6-bis(4-*tert*-butylphenyl)phenyl]perylen-3,4:9,10-bis(dicarboximide) (3a):

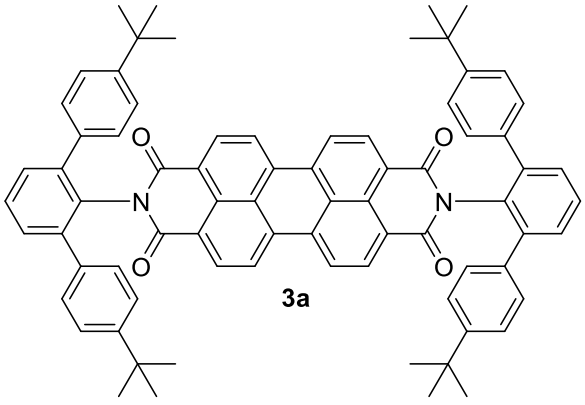

3a

2a (50.0 mg, 140 µmol, 2.0 eq.) was dissolved in THF (2 mL) under nitrogen atmosphere. The mixture was cooled down to −78 °C. Then a solution of *n*-BuLi (2.5 M, 112 µL, 280 µmol, 4.0 eq.) in hexane was added. The mixture was stirred for 1 h at this temperature. After heating to room temperature 3,4,9,10-perylenetetracarboxylic acid tetramethyl ester **1** (33.9 mg, 70.0 µmol, 1.0 eq.) was added and heated at 90 °C for 72 h. After cooling to room temperature, the crude product was concentrated under vacuum and purified by column chromatography (dichloromethane) and recrystallized in dichloromethane/methanol. The data are in agreement with the literature.[S1]

Yield: 15.1 mg (14.1 µmol, 20%) of a red crystal solid.

^{1}H-NMR (400 MHz, $C_2D_2Cl_4$, 370 K): δ/ppm = 8.37-7.86 (m, 8 H), 7.54 (t, J = 8.81 Hz, 2h), 7.45 (d, J = 7.34, 4 H), 7.25 (d, J = 7.34, 8 H), 7.09 (d, J = 8.08, 8 H), 1.01 (s, 36 H).

Synthesis of *N,N`*-Bis[2,6-bis(4-hexylphenyl)phenyl]perylen-3,4:9,10-bis(dicarboximide) (3b):

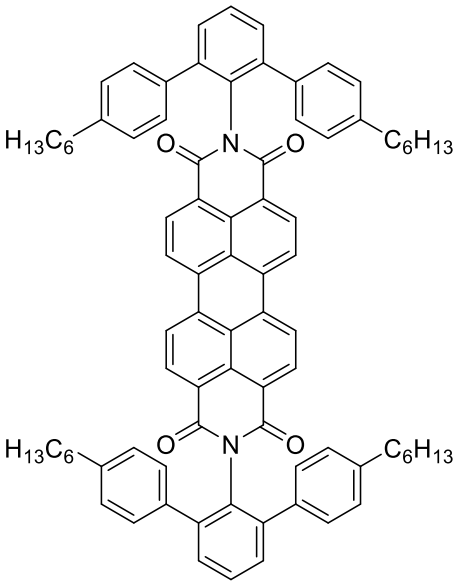

3b

2b (59.8 mg, 145 µmol, 2.0 eq.) was dissolved in THF (2 mL) under nitrogen atmosphere. The mixture was cooled down to −78 °C. Then a solution of *n*-BuLi (2.5 M, 116 µL, 289 µmol, 4.0 eq.) in hexane was added. The mixture was stirred for 1 h at this temperature. After heating to room temperature 3,4,9,10-perylenetetracarboxylic acid tetramethyl ester **1** (35.0 mg, 72.3 µmol, 1.0 eq.) was added and heated at 90 °C for 72 h. After cooling to room temperature, the crude product was concentrated under vacuum and purified by column chromatography (dichloromethane), HPLC (DCM/EtOAc = 99/1) and recrystallized in dichloromethane/methanol.

Yield: 16.5 mg (13.9 µmol, 19%) of a red crystal solid.

^{1}H-NMR (600 MHz, $C_2D_2Cl_2$, 373 K): δ/ppm = 8.29 (d, J = 7.12 Hz, 4 H), 8.24-7.95 (m, 4 H), 7.53 (t, J = 7.91 Hz, 2 H), 7.44 (d, J = 7.91 Hz, 4 H), 7.21 (d, J = 7.91 Hz, 8 H), 6.89 (d, J = 7.91 Hz, 8 H), 2.33 (t, J = 7.15 Hz, 8 H), 1.31 (quin, J = 8.17 Hz, 8 H), 1.01 (s, 24 H), 0.60 (t, J = 7.15 Hz, 12 H).

^{13}C-NMR (151 MHz, $C_2D_2Cl_2$, 373 K): δ/ppm = 163.4, 142.1, 142.0, 136.8, 134.5, 132.1, 131.2, 130.0, 129.5, 128.9, 128.6, 127.9, 126.4, 123.4, 122.8, 120.6, 35.5, 31.6, 30.9, 28.7, 22.5, 13.9.

Melting Point: 241 °C

MS (MALDI-TOF, neg. Mode, DCM): m/z calcd. for $C_{84}H_{82}N_2O_4^-$: 1182.62801; found: 1182.62844.

UV/Vis (CH_2Cl_2; 1×10^{-5} M): λ_{max}/nm (ε/$M^{-1}cm^{-1}$) = 528 (90300).

Fluorescence (CH_2Cl_2): λ_{max}/nm = 535.

Synthesis of *N,N`*-Bis[2,6-bis(4-(1-pentylhexyl)phenyl)phenyl]perylene-3,4:9,10-bis(dicarboximide) (**3c**):

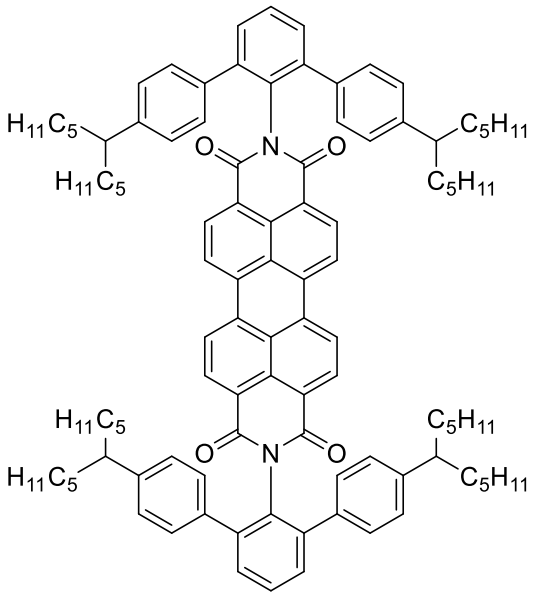

3c

2c (80.0 mg, 144 µmol, 1.0 eq.) was dissolved in THF (2 mL) under nitrogen atmosphere. The mixture was cooled down to −78 °C. Then a solution of *n*-BuLi (2.5 M, 116 µL, 289 µmol, 4.0 eq.) in hexane was added. The mixture was stirred for 1 h at this temperature. After heating to room temperature 3,4,9,10-perylenetetracarboxylic acid tetramethyl ester **1** (35.0 mg, 72.3 µmol, 1.0 eq.) was added and heated at 90 °C for 72 h. After cooling to room temperature, the crude product was concentrated under vacuum and purified by column chromatography (dichloromethane/cyclohexane = 1/1).

Yield: 3.17 mg (2.17 µmol, 3%) of a red solid.

^{1}H-NMR (400 MHz, $CDCl_3$, 298 K): δ/ppm = 8.41 (s, 8H), 7.60 (t, *J* = 8.91 Hz, 2H), 7.53 (d, *J* = 8.39 Hz, 4H), 7.23 (d, *J* = 8.39 Hz, 8H), 6.87 (d, *J* = 7.87 Hz, 8H), 2.25 (sep., *J* = 5.77 Hz, 4H), 1.40-1-19 (m, 16H), 0.96-0.65 (m, 48H), 0.56-0.50 (m, 24H).

^{13}C-NMR (100 MHz, $C_2D_2Cl_2$, 373 K): δ/ppm = 163.4, 145.3, 141.8, 136.6, 134.6, 131.6, 131.4, 129.9, 129.4, 128.2, 127.2, 126.3, 122.9, 122.7, 45.6, 36.8, 31.9, 27.1, 22.5, 14.1.

Melting Point: 198 °C

MS (MALDI-TOF, pos. Mode, DCM): *m/z* calcd. for $C_{104}H_{122}N_2O_4Na$: 1485.93023; found 1485.93128 $[M+Na]^+$.

UV/Vis (CH_2Cl_2; 1×10^{-5} M): λ_{max}/nm (ε/$M^{-1}cm^{-1}$) = 528 (89200).

Fluorescence (CH_2Cl_2): λ_{max}/nm = 534.

3. UV/Vis and fluorescence spectroscopy

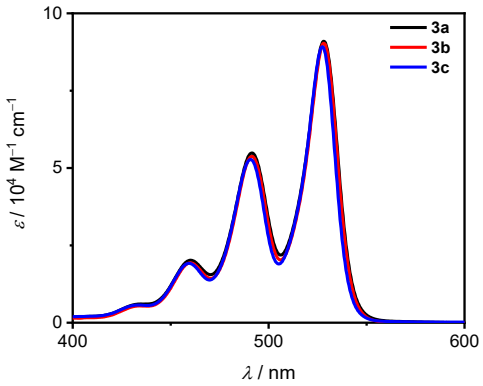

Fig. S1 UV/Vis absorption spectra of PBI **3a** (black), **3b** (red) and **3c** (blue in DCM solution (c_0 = 1×10^{-5} M) at room temperature.

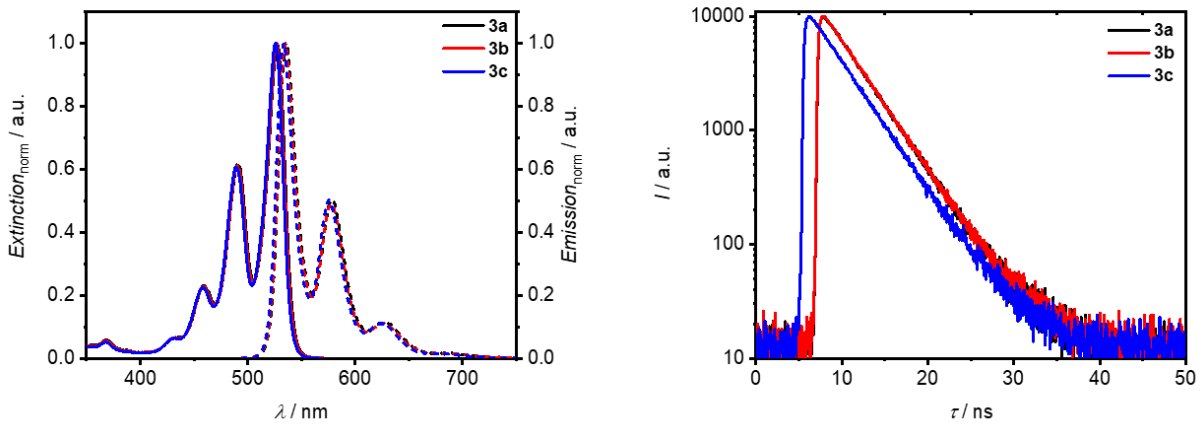

Fig. S2 Normalised UV/Vis absorption (solid line) and fluorescence (dashed line) spectra of PBIs **3a** (black), **3b** (red) and **3c** (blue) in DCM solution (c_0 = 4.5 × 10^{-7} M) at room temperature. Emission spectra were recorded with excitation at λ_{ex} = 489 nm and lifetime measurements with excitation at 505.8 nm while detecting at 578 nm.

Tab. S1 Optical properties of the PBIs **3a**-**3c** in DCM at room temperature.

PBI	λ_{abs}^{Lsg} / nm	ε_{max} / M^{-1} cm^{-1}	A_{00}/A_{01} / 1	λ_{em}^{Lsg} / nm	$\Delta\tilde{\nu}_{Stokes}$ /cm^{-1}	Φ_{fl} [a] / %	τ [b] / ns	χ^2 / 1
3a	528, 491	91100	1.66	536, 578	280	97 ± 1	3.85 ± 0.01	1.256
3b	528, 492	90300	1.68	535, 578	250	97 ± 2	3.86 ± 0.01	1.205
3c	528, 491	89200	1.69	534, 576	280	94 ± 1	3.88 ± 0.01	1.332

[a] Fluorescence quantum yields were determined using the relative method (A < 0.05) and *N*,*N*′-bis(2,6-diisopropylphenyl) perylene-3,4:9,10-bis(dicarboxmide) ($\Phi_{fl}(CHCl_3)$ = 100%) as reference.[S6] [b] λ_{ex} = 505.8 nm.

4. Aggregation studies

Tab. S2 Dimerization constants (K / M^{-1}) as well as Gibbs free energies (ΔG^0 / kJ mol^{-1}) of the PBIs **3a**-**c** in the solvents $CHCl_3$, TCE and MCH at 298 K. The constants were obtained by single wavelength fit at the PBIs respective UV/Vis absorption maximum.

	$CHCl_3$		TCE		MCH	
PBI	K	ΔG^0	K	ΔG^0	K	ΔG^0
3a	870 ± 140	−16.8	n.d.	-	n.d.[a]	-
3b	140 ± 13	−12.2	100 ± 11	−11.4	43000 ± 1300	−26.4
3c	-[b]	-	-[b]	-	-[b]	-

[a] Not measured due to bad solubility. [b] Does not show signs of aggregation.

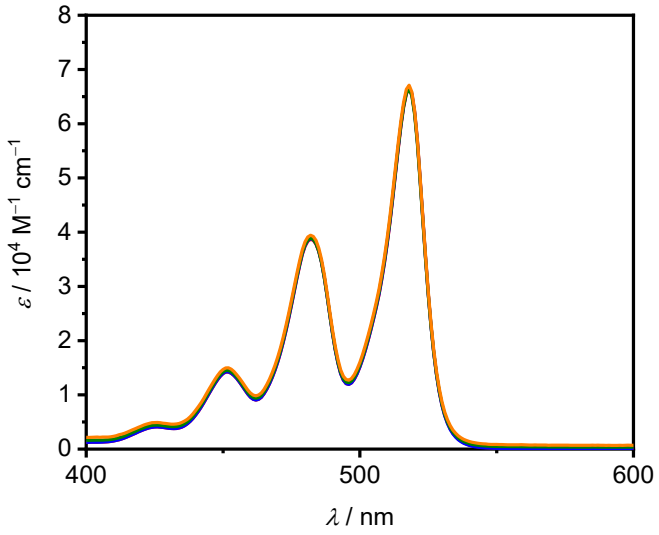

Fig. S3 Concentration-dependent UV/Vis absorption spectra of an aggregation study of PBI **3c** in MCH with a concentration of 1.45×10^{-4} M (red), 1.43×10^{-5} M (blue), 1.49×10^{-6} M (green) and 5.19×10^{-7} M (orange).

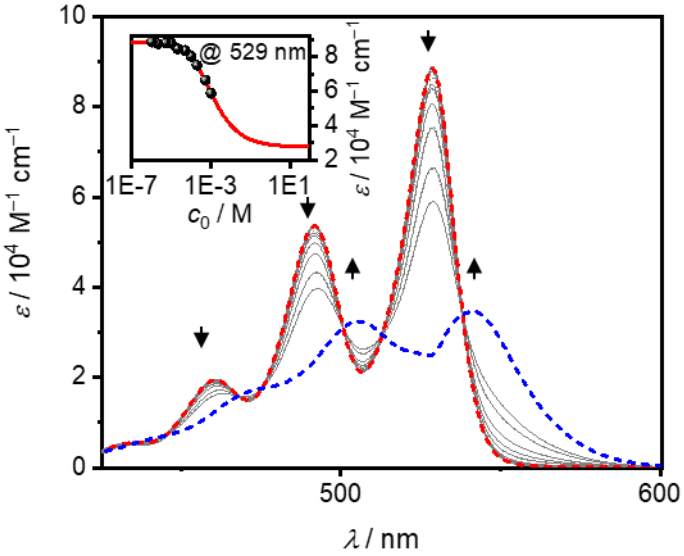

Fig. S4 Concentration-dependent UV/Vis absorption spectra (grey solid lines) of an aggregation study of PBI **3a** in $CHCl_3$ (c_0 = 1 × 10^{-3} - 1 × 10^{-6} M) at 298 K. The dashed lines represent the calculated monomer (red) and dimer (blue) absorption spectra according to a global fit analysis by the monomer-dimer model. The arrows indicate the spectral changes with increasing concentration. The inset depicts the local monomer-dimer fit (red line) at λ_{max} = 529 nm of the experiment (black symbols).

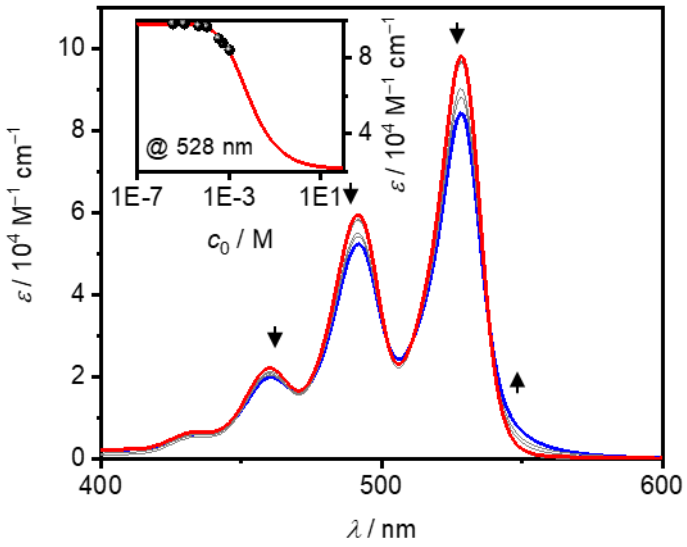

Fig. S5 Concentration-dependent UV/Vis absorption spectra of an aggregation study of PBI **3b** in $CHCl_3$ (c_0 = 1 × 10^{-3} - 3.6 × 10^{-6} M) at 298 K. The red line represents the start and the blue line the end of the measurement. The arrows indicate the spectral changes with increasing concentration. The inset depicts the single wavelength monomer-dimer fit (red line) at λ_{max} = 528 nm of the experiment (black symbols). The single wavelength fit was performed with a fixed extinction coefficient for the dimer of 21151 M^{-1} cm^{-1}.

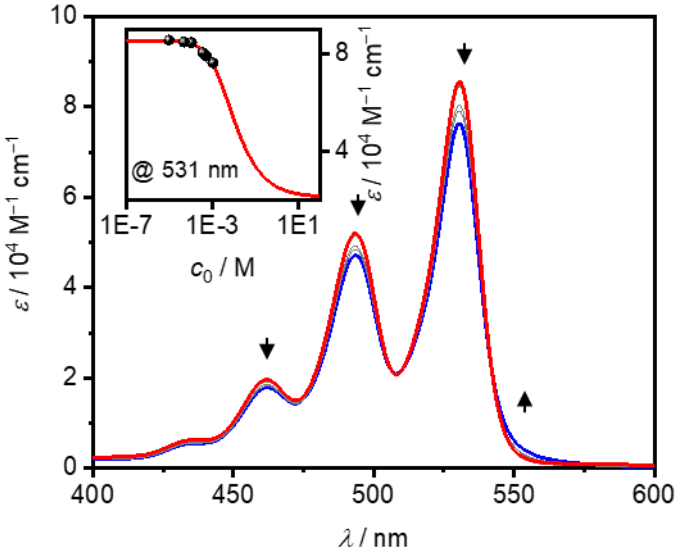

Fig. S6 Concentration-dependent UV/Vis absorption spectra of an aggregation study of PBI **3b** in TCE (c_0 = 1 × 10^{-3} - 9.2 × 10^{-6} M) at 298 K. The red line represents the start and the blue line the end of the measurement. The arrows indicate the spectral changes with increasing concentration. The inset depicts the single wavelength monomer-dimer fit (red line) at λ_{max} = 529 nm of the experiment (black symbols). The single wavelength fit was performed with a fixed extinction coefficient for the dimer of 21151 M^{-1} cm^{-1}.

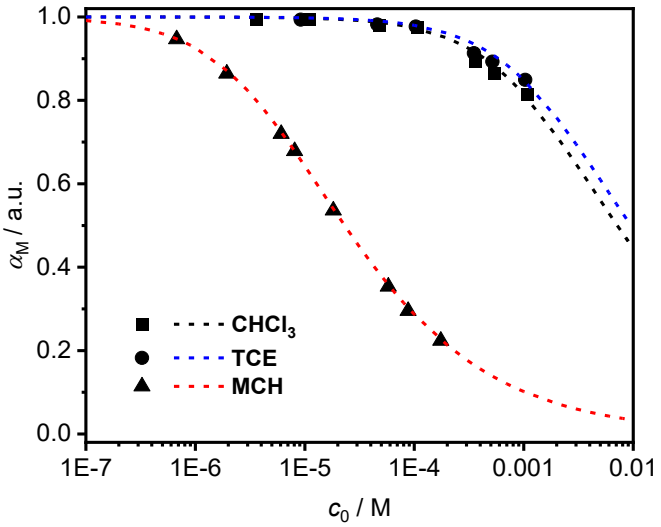

Fig. S7 Comparison of the degree of aggregation (α_M= 1 – α_{Agg}) of PBI **3b** in $CHCl_3$ (black, square), TCE (blue, circle) and MCH (red, triangle) as estimated from the values ε_M and ε_D determined from the fit parameters in MCH.

5. Single crystal X-ray analysis

Tab. S3 Crystallographic data and structure refinements for PBI single crystals and co-crystals.

	3a[a]	**3b**	[P·**3a**·P]	[T·**3a**·T]
Empirical formula	$C_{83}H_{74}N_2O_4$	$C_{84.13}H_{82.54}N_2O_{4.13}$	$C_{130}H_{106}N_2O_4$	$C_{112}H_{90}N_2O_4$
$M_{empirical}$ (g mol^{-1})	1163.44	1187.80	1760.16	1527.85
Wavelength (Å)	1.54178	1.54178	1.54178	1.54178
T (K)	100	100	100	100
Description of the crystal:				
Color	Red	Red	Green	Red
Habit	Block	Block	Needle	Needle
Crystal System	Triclinic	Triclinic	Monoclinic	Orthorhombic
Space group	P$\bar{1}$	P$\bar{1}$	P $2_1/n$	$P2_12_12_1$
Unit cell dimension				
a (Å)	16.5447(14)	16.7684(6)	19.1429(12)	13.0958(19)
b (Å)	18.7892(16)	28.0025(11)	12.7014(8)	22.198(3)
c (Å)	23.3659(19)	29.4188(10)	19.3268(13)	27.902(3)
α (°)	82.920(4)	79.520(2)	90	90
β (°)	83.513(4)	87.831(2)	101.922(2)	90
γ (°)	77.185(4)	73.246(2)	90	90
Volume (Å^3)	7001.1(10)	13005.2(8)	4597.8(5)	8111.1(19)
Z	4	8	2	4
$\rho_{alc.}$ (g cm^{-3})	1.104	1.213	1.271	1.251
F(000)	2472.0	5075.3	1864.0	3232.0
Goodness of Fit	1.077	1.028	1.028	1.048
CCDC	2284853	2284854	2284855	2284856

[a] The PLATON SQUEEZE program was used to remove the contributions of disordered solvent molecules.[S11-S12]

Details on the content of each asymmetric unit of the described single crystal structures in Table S3:

3a: The asymmetric unit has two **3a** molecules and two disordered toluene molecules, one with partial-occupancy values of 0.512(8) and 0.488(8) and the other with partial-occupancy values of 0.121(3), 0.370(3) and 0.510(3).

3b: The asymmetric unit has four **3b** molecules and two methanol molecules with partial-occupancy values of 0.201(6) and 0.336(6).

[P·**3a**·P]: The asymmetric unit has half of molecule **3a** (with some minor disorder of *t*Bu groups), one disordered perylene molecule with partial-occupancy values of 0.471(15) and 0.529(15), as well as one disordered molecule of toluene with partial-occupancy values of 0.517(3), 0.287(3) and 0.196(3).

[T·**3a**·T]: The asymmetric unit has one molecule of **3a** (with some minor disorder of *t*Bu groups) and two triphenylene molecules, one fully occupied and the other one disordered with partial-occupancy values of 0.596(9) and 0.404(9).

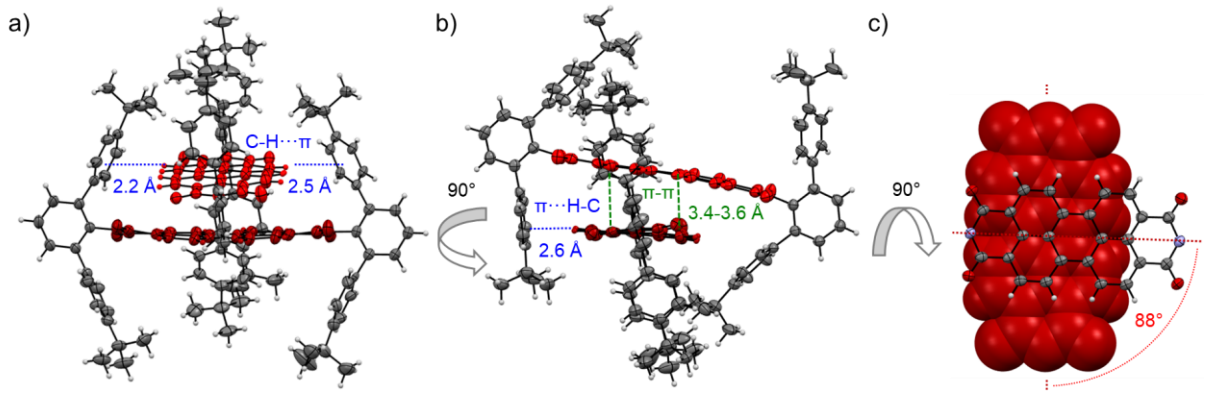

Fig. S8 Molecular packing of PBI **3a** in dimeric π-stacks in the single crystals grown from toluene and *n*-hexane in side (a,b) as well as top (c) view onto the PBIs π-system. C-H···π (blue) and π-π (green) interactions as well as the rotational displacement (red) between the PBI´s *N*,*N*´-axes are indicated. Ellipsoids are set to 50% probability and the PBI chromophores are highlighted in red. Solvent molecules and molecular disorder are omitted for clarity.

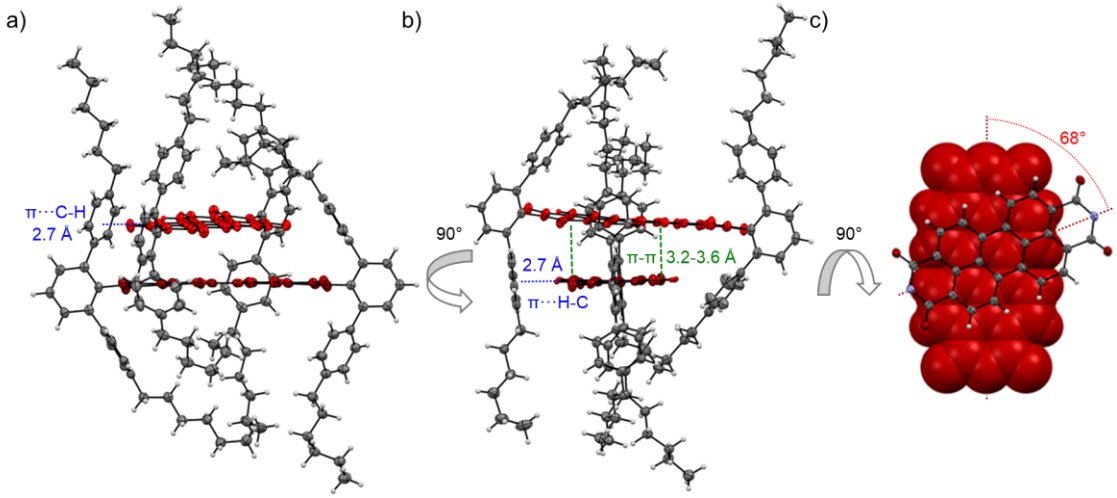

Fig. S9 Molecular packing of PBI **3b** in dimeric π-stacks in the single crystals grown from toluene and *n*-hexane in side (a,b) as well as top (c) view onto the PBIs π-system. C-H···π (blue) and π-π (green) interactions as well as the rotational displacement (red) between the PBI´s *N*,*N*´-axes are indicated. Ellipsoids are set to 50% probability and the PBI chromophores are highlighted in red. Solvent molecules and molecular disorder are omitted for clarity.

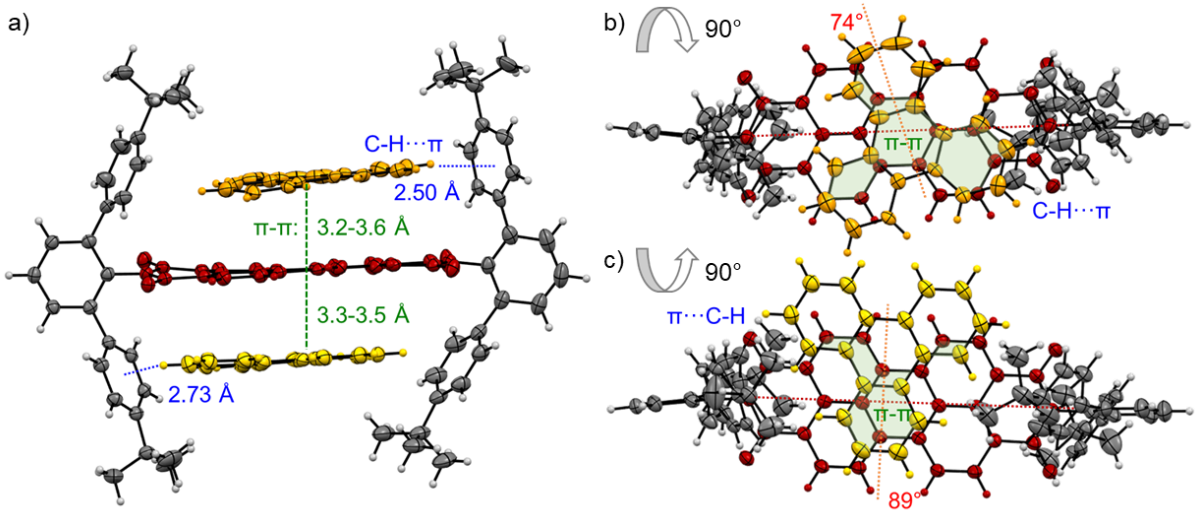

Fig. S10 Structure of the 1:2 complex of PBI **3a** (red) with two triphenylene guest molecules (orange, yellow) as observed by X-ray diffraction of single crystals grown from toluene and methanol in side (a) as well as top (b,c) view onto the PBIs π-system. C-H···π (blue) and π-π (green) interactions as well as the rotational displacements (red) between the PBIs *N*,*N*´-axis and each guest molecule are indicated. Ellipsoids are set to 50% probability and solvent molecules as well as molecular disorder are omitted for clarity.

6. Theoretical calculations (dimers)

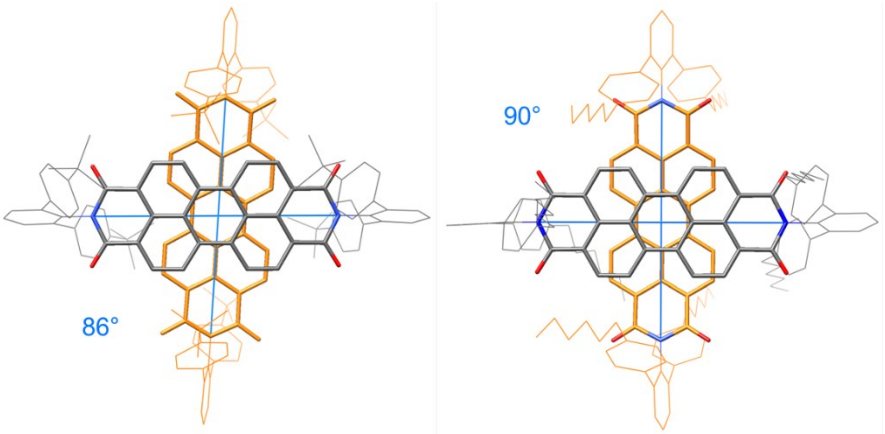

Fig. S11 Optimized geometries of dimers of **3a** (left) and **3b** (right) obtained from docking derived from the single crystal structure after geometry optimization by ORCA 5.0.4 [S26] at the r^2-SCAN-3c level.

Tab. S4 Calculated exciton coupling energies and effective hole/electron transfer integrals for dimers of **3a** and **3b**.

		3a (86°)	**3b** (90°)
J	cm^{-1}	−273	−12
J_{Coul}	cm^{-1}	94	−7
t_e	cm^{-1}	349	6
t_h	cm^{-1}	843	757
J_{CT}	cm^{-1}	−367	−5

7. Complexation studies

All UV/Vis absorption spectra of the PBI **3a**-**c** titration studies with perylene and triphenylene are available in the Zenodo repository DOI: https://doi.org/10.5281/zenodo.8196841.

Tab. S5 Binding constants (K / M^{-1}) as well as Gibbs free energies (ΔG^0 / kJ mol^{-1}) of the PBIs **3a**-**c** in TCE with perylene (P) as well as triphenylene (T) as guest molecules determined by UV/Vis titration experiments at 298 K. The constants were obtained, were possible, by global 1:1 and 1:2 fit (500-550 nm). All binding constants reported are within 0.5 kJ mol^{-1} of error in ΔG^0. Similar global bindfit analyses for titration studies in $CHCl_3$ and MCH were only performed with the 1:1 binding model due to insufficient solubility of the guest molecules in the respective solvent. K_1 values are provided in each Figure.

Sol.	**Perylene (P)**				**Triphenylene (T)**			
PBI (Fit)	K_1[a]	$\Delta G_1{}^0$	K_2[a]	$\Delta G_2{}^0$	K_1[a]	$\Delta G_1{}^0$	K_2[a]	$\Delta G_2{}^0$
3a (1:1)	219	−13.3	-		81	−10.9	-	-
3a (1:2)	254	−13.7	23	−7.8	81	−10.9	13	−6.4
3b (1:1)	84	−11.0	-		42	−9.3	-	-
3b (1:2)	135	−12.1	12	−6.2	56	−10.0	9	−5.4
3c (1:1)	10	−5.7	-	-	11	−5.9	-	-
3c (1:2)	- [b]	-	- [b]	-	- [b]	-	- [b]	-

[a] Error of < ±2.0% as determined by bindfit global analysis; [b] unreliable fitting results.

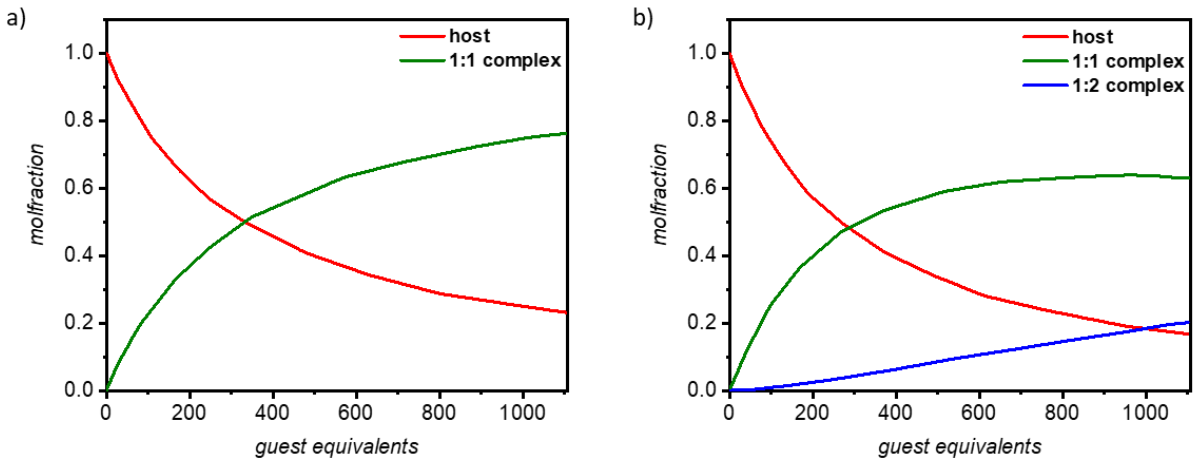

Fig. S12 a) Molar fractions of free host (red) and 1:1 complex (green) according to global fit (500-550 nm) in 1:1 model and b) molar fractions of free host (red), 1:1 complex (green) and 1:2 complex (blue) according to global fit (500-550 nm) in 1:2 model for the UV/Vis complexation study of **3a** with perylene as guest in TCE at 298 K shown in Fig. 3.

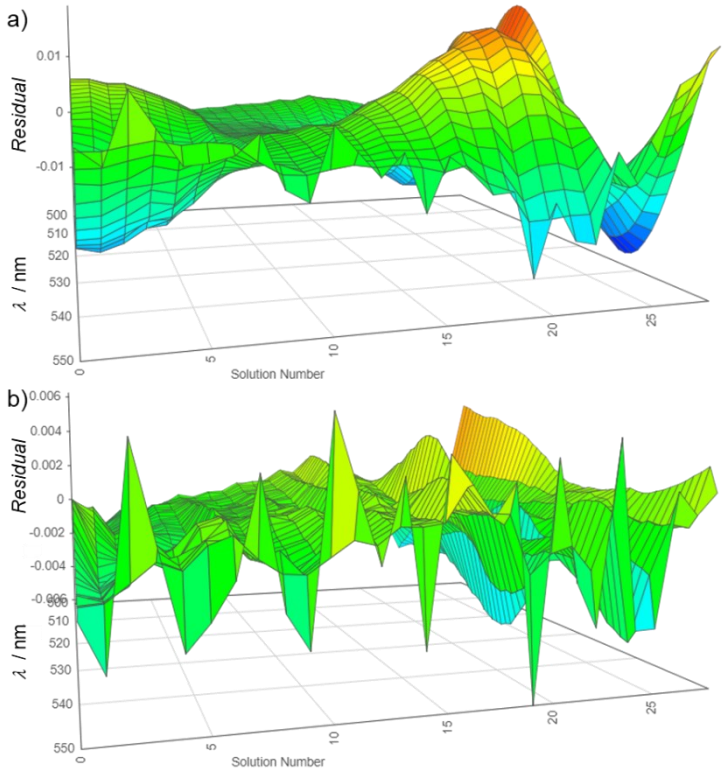

Fig. S13 Residual analysis of the global (500-550 nm) fitting with a) 1:1 and b) 1:2 binding models using the program SIVVU[S27] for the UV/Vis absorption spectra of a solution of PBI **3a** as host ($c_0 = 1.34 \times 10^{-5}$ M) and changes upon addition of perylene as guest in TCE at 298 K.

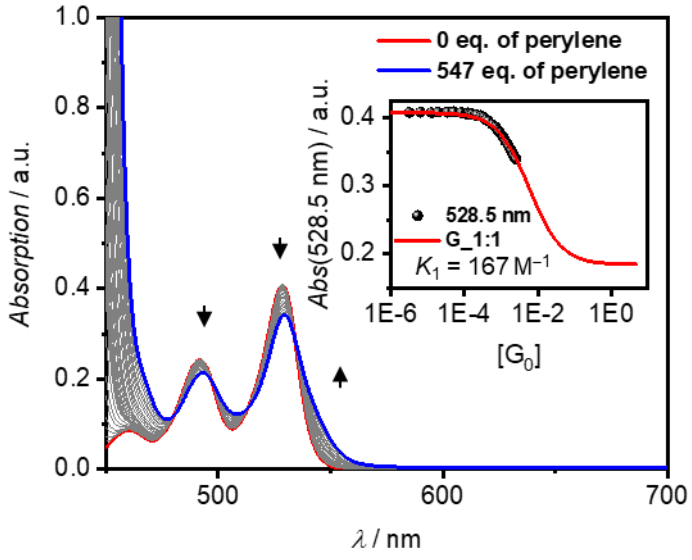

Fig. S14 UV/Vis absorption spectra (solid lines) for a solution of PBI **3a** as host ($c_0 = 4.66 \times 10^{-6}$ M, red line) and changes upon addition of perylene as guest (grey, 547 eq. blue line) in $CHCl_3$ at 298 K. Arrows depict the spectral changes with increasing equivalents (eq.) of the guest perylene. Inset: Resulting plot of the absorption at λ_{max} = 528.5 nm (black symbol) with nonlinear curve fit by the 1:1 (red line) global (500-550 nm) binding model.

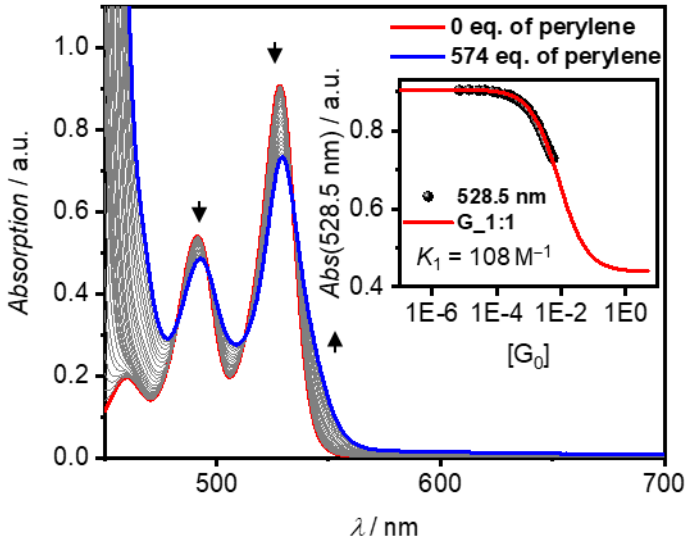

Fig. S15 UV/Vis absorption spectra (solid lines) for a solution of PBI **3b** as host ($c_0 = 1.01 \times 10^{-5}$ M, red line) and changes upon addition of perylene as guest (grey, 574 eq. blue line) in $CHCl_3$ at 298 K. Arrows depict the spectral changes with increasing equivalents (eq.) of the guest perylene. Inset: Resulting plot of the absorption at $\lambda_{max} = 528.5$ nm (black symbol) with nonlinear curve fit by the 1:1 (red line) global (500-550 nm) binding model.

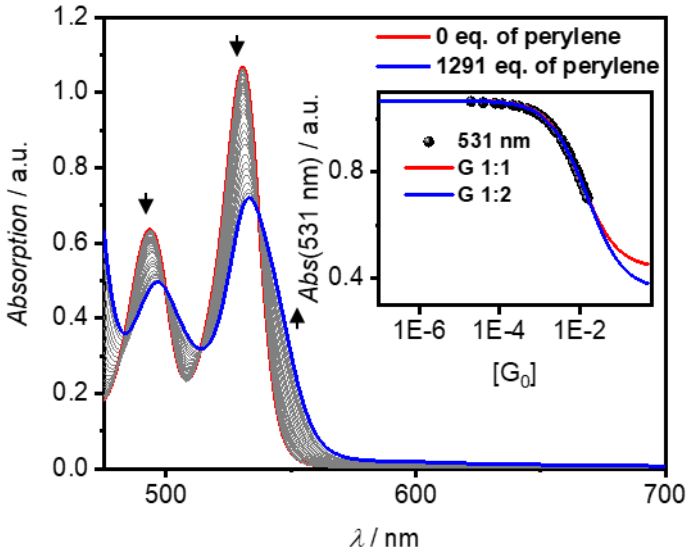

Fig. S16 UV/Vis absorption spectra (solid lines) for a solution of PBI **3b** as host ($c_0 = 1.20 \times 10^{-5}$ M, red line) and changes upon addition of perylene as guest (grey, 1291 eq. blue line) in TCE at 298 K. Arrows depict the spectral changes with increasing equivalents (eq.) of the guest perylene. Inset: Resulting plot of the absorption at $\lambda_{max} = 531$ nm (black symbol) with nonlinear curve fits by the 1:1 (red line) and 1:2 (blue line) global (500-550 nm) binding models.

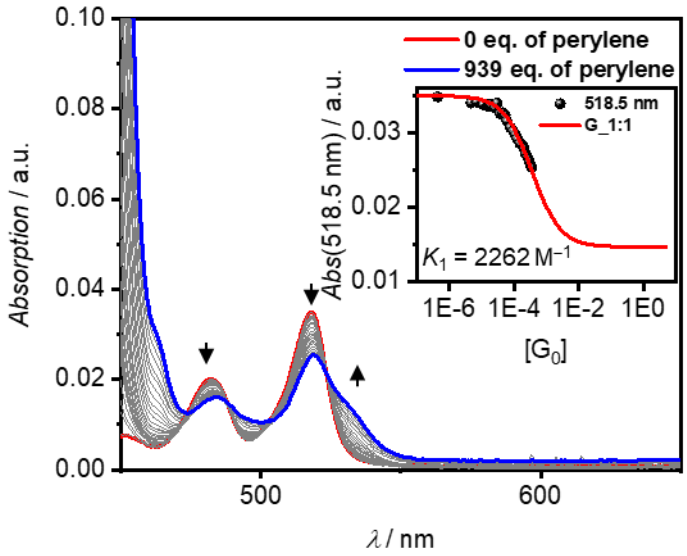

Fig. S17UV/Vis absorption spectra (solid lines) for a solution of PBI **3b** as host ($c_0 = 3.79 \times 10^{-7}$ M, red line) and changes upon addition of perylene as guest (grey, 939 eq. blue line) in MCH at 298 K. Arrows depict the spectral changes with increasing equivalents (eq.) of the guest perylene. Resulting plot of the absorption at λ_{max} = 518.5 nm (black symbol) with nonlinear curve fit by the 1:1 (red line) global (500-550 nm) binding model.

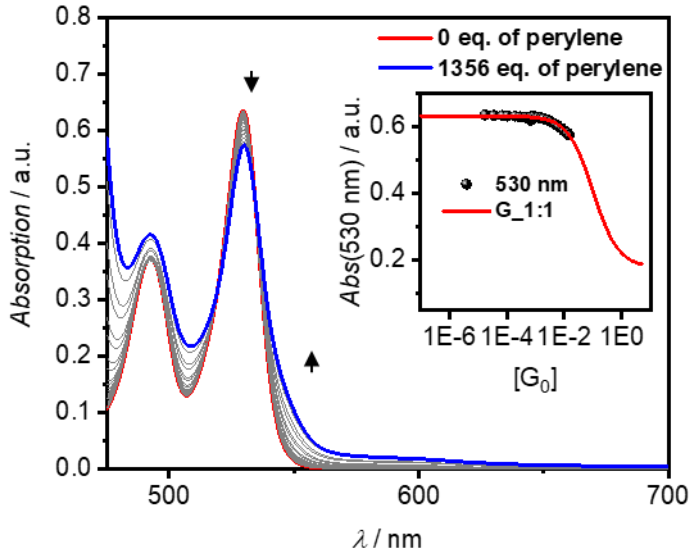

Fig. S18 UV/Vis absorption spectra (solid lines) for a solution of PBI **3c** as host ($c_0 = 7.17 \times 10^{-6}$ M, red line) and changes upon addition of perylene as guest (grey, 1356 eq. blue line) in TCE at 298 K. Arrows depict the spectral changes with increasing equivalents (eq.) of the guest perylene. Inset: Resulting plot of the absorption at λ_{max} = 518.5 nm (black symbol) with nonlinear curve fit by the 1:1 (red line) global (500-550 nm) binding model.

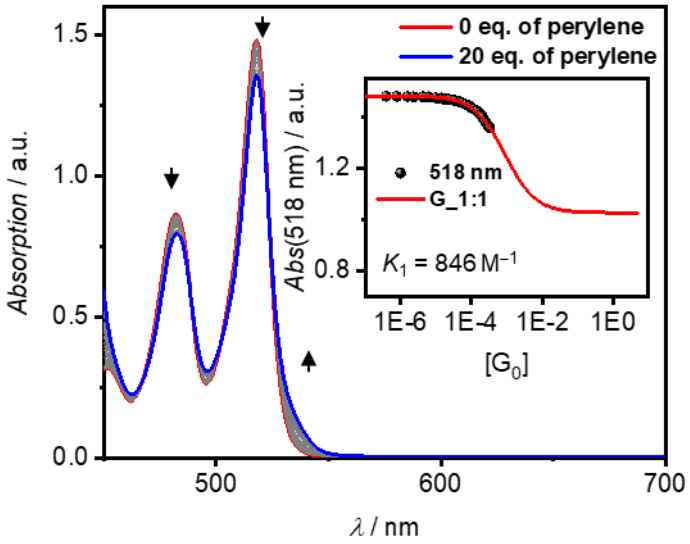

Fig. S19 UV/Vis absorption spectra (solid lines) for a solution of PBI **3c** as host ($c_0 = 1.65 \times 10^{-5}$ M, red line) and changes upon addition of perylene as guest (grey, 20 eq. blue line) in MCH at 298 K. Arrows depict the spectral changes with increasing equivalents (eq.) of the guest perylene. Inset: Resulting plot of the absorption at λ_{max} = 518 nm (black symbol) with nonlinear curve fit by the 1:1 (red line) global (500-550 nm) binding model.

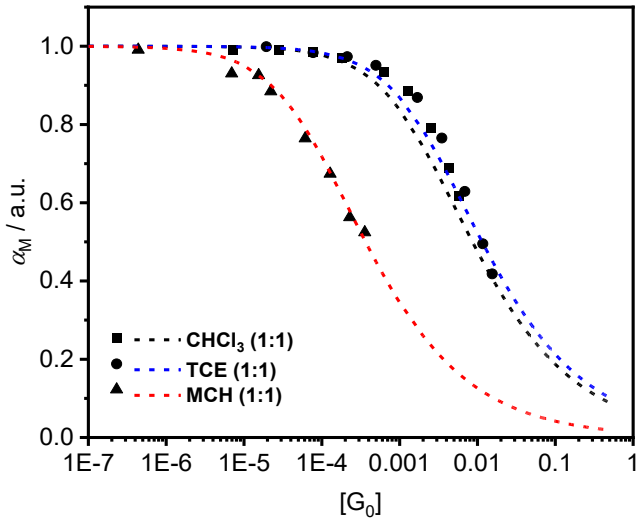

Fig. S20 Comparison of the degree of complexation ($\alpha_M = 1 - \alpha_C$) of PBI host **3b** with guest perylene (P) in $CHCl_3$ (black, square), TCE (blue, circle) and MCH (red, triangle) as estimated from the values ε_M and ε_{com} determined from the 1:1 fit parameters.[S7,S8]

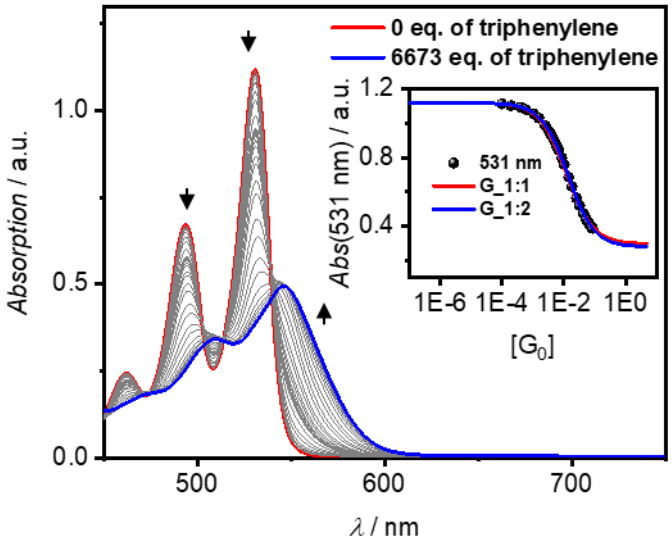

Fig. S21 UV/Vis absorption spectra (solid lines) for a solution of PBI **3a** as host ($c_0 = 1.26 \times 10^{-5}$ M, red line) and changes upon addition of triphenylene as guest (grey, 6673 eq. blue line) in TCE at 298 K. Arrows depict the spectral changes with increasing equivalents (eq.) of the guest triphenylene. Inset: Resulting plot of the absorption at λ_{max} = 531 nm (black symbol) with nonlinear curve fits by the 1:1 (red line) and 1:2 (blue line) global (500-550 nm) binding models.

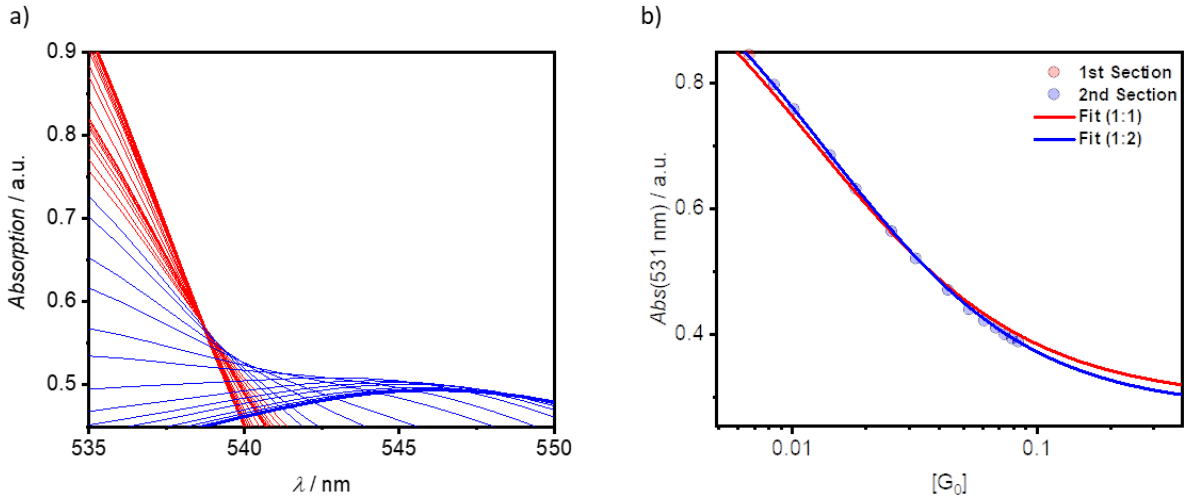

Fig. S22 a) Zoom in of the UV/Vis titration study of **3a** with triphenylene at 298 K, shown in Fig. S21. The red spectra show that an isosbestic point is present after a certain addition of guest, but after further addition (blue lines) the isosbestic point is lost. b) The fits also show, that the 1:2 fit corresponds better with the experimental data than the 1:1 fit.

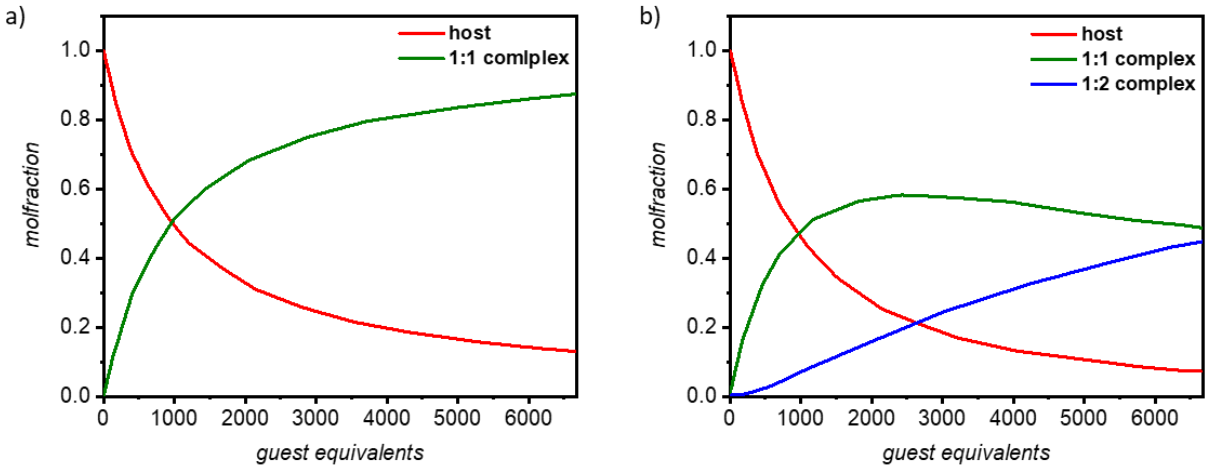

Fig. S23 Molar fractions of free host (red) and 1:1 complex (green) according to global fit (500-550 nm) in 1:1 model (a) and molar fractions of free host (red), 1:1 complex (green) and 1:2 complex (blue) according to global fit (500-550 nm) in 1:2 model for the UV/Vis complexation study of **3a** with triphenylene in TCE at 298 K shown in Fig. S21.

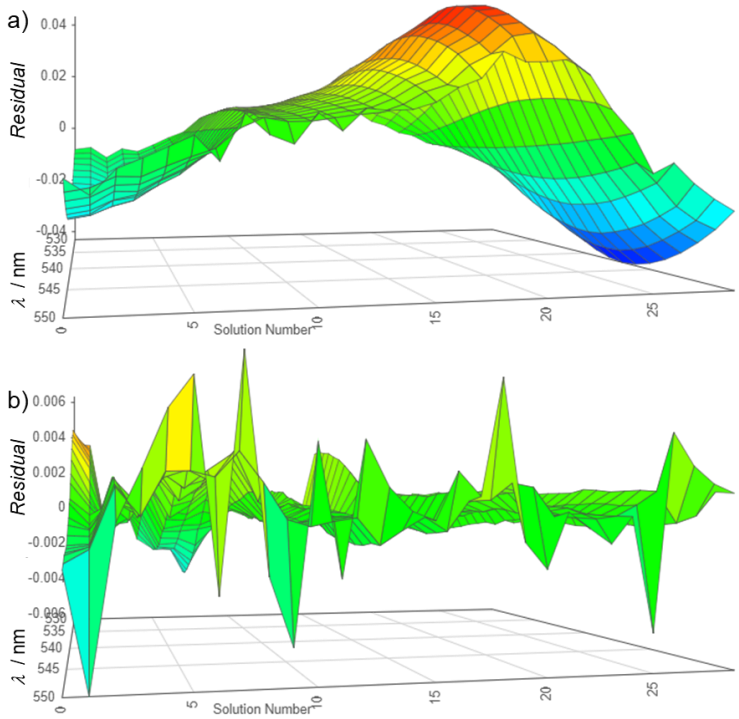

Fig. S24 Residual analysis of the global (500-550 nm) fitting with a) 1:1 and b) 1:2 binding models using the program SIVVU[S27] for the UV/Vis absorption spectra of a solution of PBI **3a** as host ($c_0 = 1.26 \times 10^{-5}$ M) and changes upon addition of triphenylene as guest in TCE at 298 K.

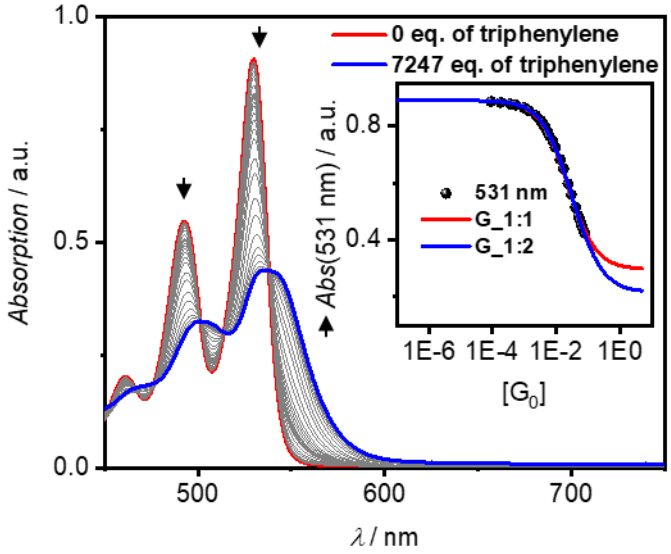

Fig. S25 UV/Vis absorption spectra (solid lines) for a solution of PBI **3b** as host ($c_0 = 1.09 \times 10^{-5}$ M, red line) and changes upon addition of triphenylene as guest (grey, 7247 eq. blue line) in TCE at 298 K. Arrows depict the spectral changes with increasing equivalents (eq.) of the guest triphenylene. Inset: Resulting plot of the absorption at λ_{max} = 531 nm (black symbol) with nonlinear curve fits by the 1:1 (red line) and 1:2 (blue line) global (500-550 nm) binding models.

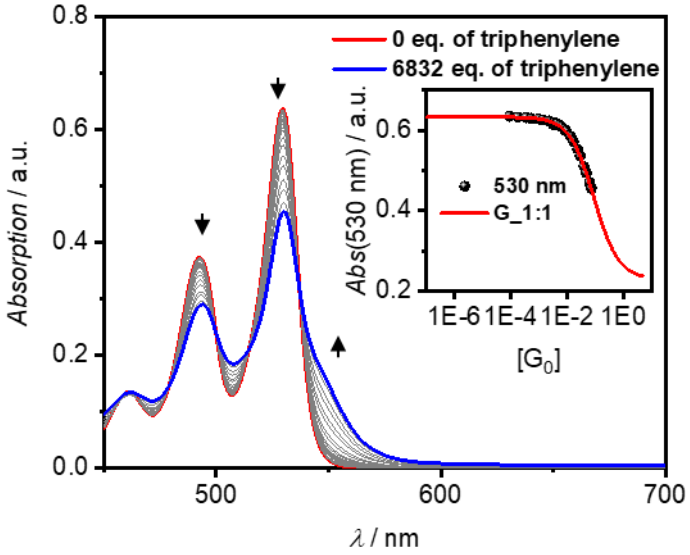

Fig. S26 UV/Vis absorption spectra (solid lines) for a solution of PBI **3c** as host ($c_0 = 7.10 \times 10^{-6}$ M, red line) and changes upon addition of triphenylene as guest (grey, 6832 eq. blue line) in TCE at 298 K. Arrows depict the spectral changes with increasing equivalents (eq.) of the guest triphenylene. Inset: Resulting plot of the absorption at λ_{max} = 530 nm (black symbol) with nonlinear curve fit by the 1:1 (red line) global (500-550 nm) binding model.

Tab. S6 Binding constants (K / M^{-1}) as well as Gibbs free energies (ΔG^0 / kJ mol^{-1}) of the PBI **3a** in the solvent TCE with perylene (P) and triphenylene (T) as guest molecules determined by fluorescence titration experiments at 298 K (Fig. S27). The constants were obtained by global 1:1 and 1:2 fit (538-650 nm).[a] All binding constants reported are within 0.5 kJ mol^{-1} of error in ΔG^0.

	Perylene (P)				Triphenylene (T)			
PBI	K_1[b]	$\Delta G_1{}^0$	K_2[b]	$\Delta G_2{}^0$	K_1[b]	$\Delta G_1{}^0$	K_2[b]	$\Delta G_2{}^0$
3a (1:1)	337	−14.4	-	-	111	−11.7	-	-
3a (1:2)	285	−14.0	61	−10.2	106	−11.5	10	−5.7

[a] Due to dynamic quenching processes fluorescence titration values are less reliable than those derived from UV/Vis absorption studies. [b] Error of < ±2.3% as determined by bindfit global analysis.

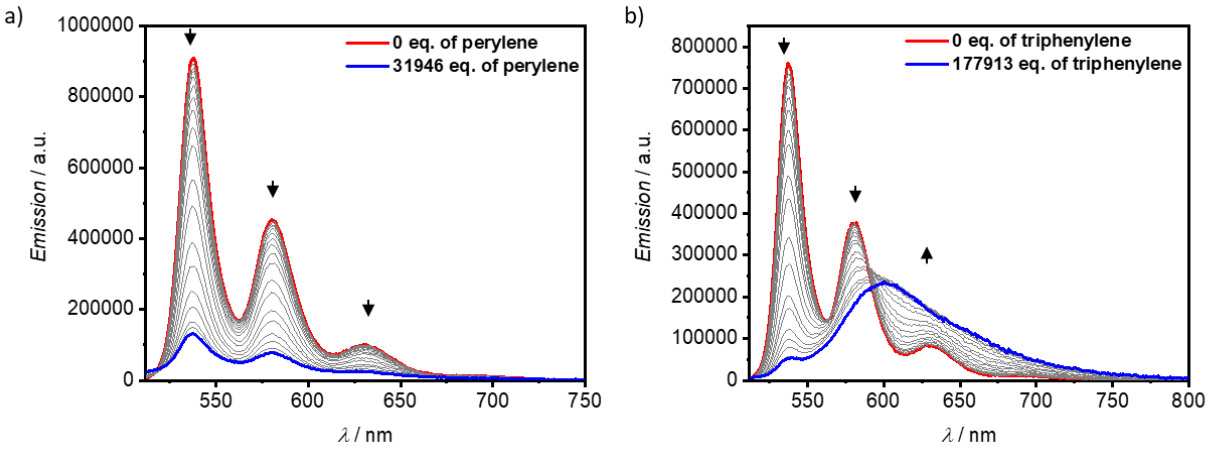

Fig. S27 Fluorescence spectra (solid lines) for a solution of PBI **3a** as host (c_0 = 4.62 × 10^{-7} M, red line) and changes upon addition of a) perylene or b) triphenylene as guest (grey, max. eq. blue line) in TCE at 298 K. Arrows depict the spectral changes with increasing equivalents (eq.) of the guests. Emission spectra were recorded with excitation at λ_{ex} = 500.5 nm.

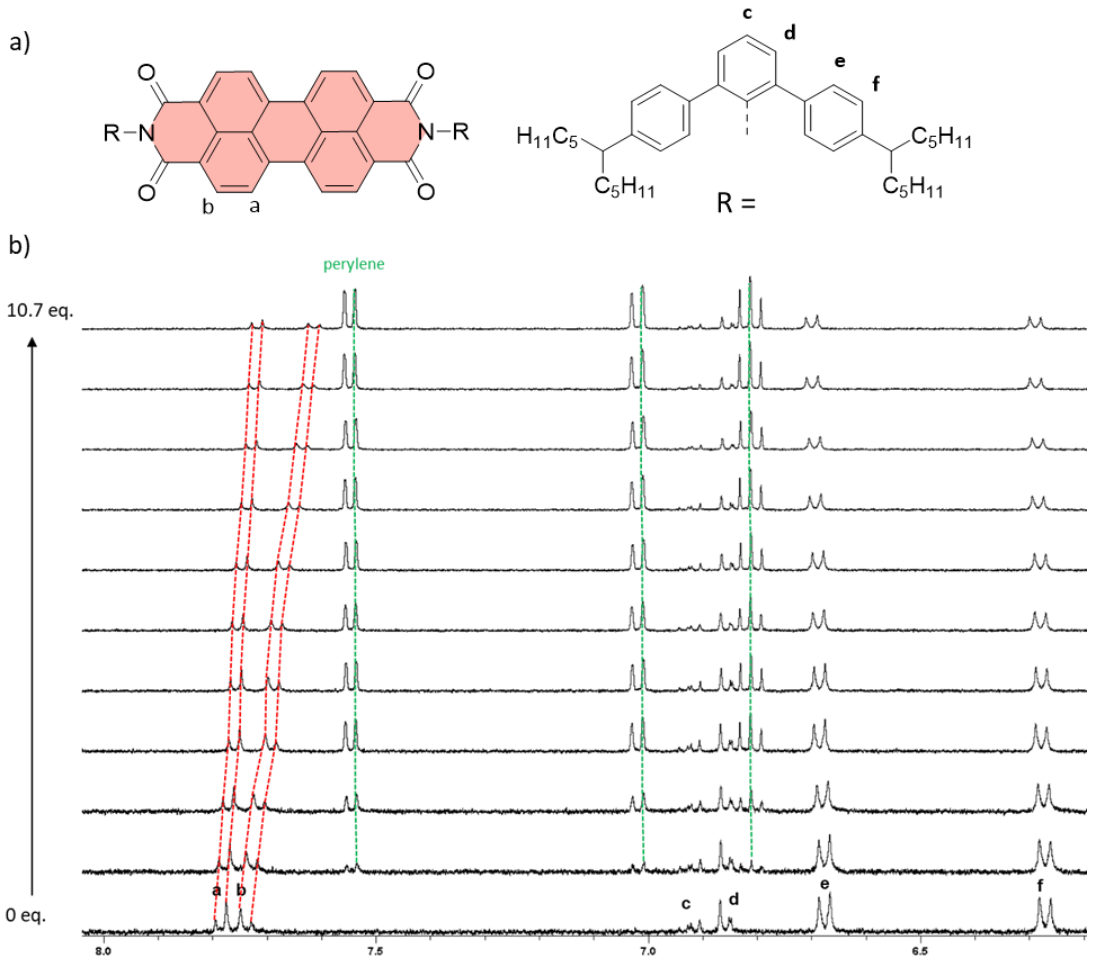

Fig. S28 Chemical structure of the PBI **3c** (a). Excerpts of ^{1}H NMR titration study of PBI **3c** as host ($c_0 = 7.69 \times 10^{-5}$ M, d^{14}-MCH, 298 K, 400 MHz) and changes upon addition of perylene as guest (10.7 eq.) (b). Green line represents the perylene signals after further addition and red line the changes of the PBI-core signals (**a**, **b**) after further addition (1:1 model: $K_1 = 725$ M^{-1}).

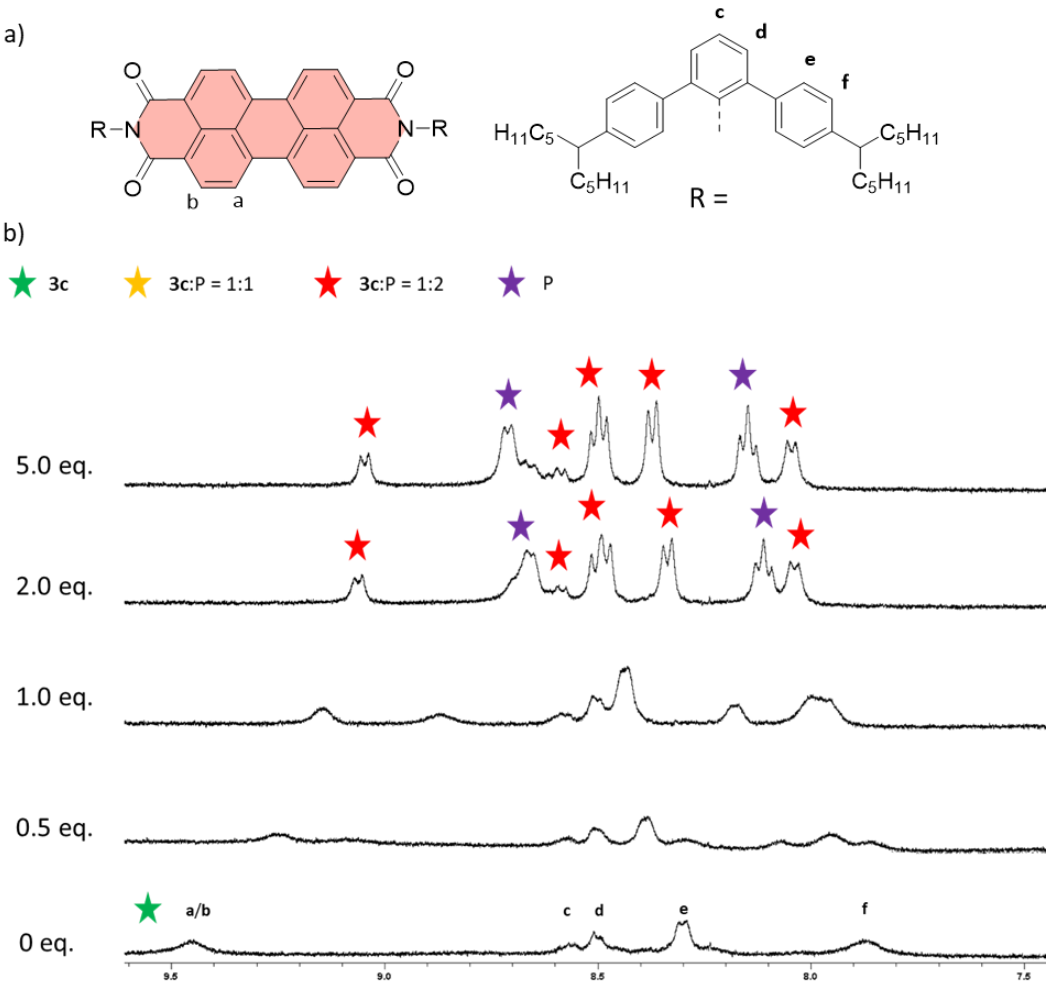

Fig. S29 Chemical structure of the PBI **3c** (a). Excerpts of low-temperature ^{1}H NMR titration study of PBI **3c** as host ($c_0 = 3 \times 10^{-4}$ M, d^{14}-MCH, 223 K, 400 MHz) and changes upon addition of perylene as guest (5 eq.) (b). Green star represents the pure host. After addition of 0.5 and 1.0 eq. of perylene the signals are broadening. After addition of 2.0 eq. the signals get sharper (red star). After further addition of 5 eq. the perylene signal increases (purple star).

8. Microscopy and spectroscopy of single crystals

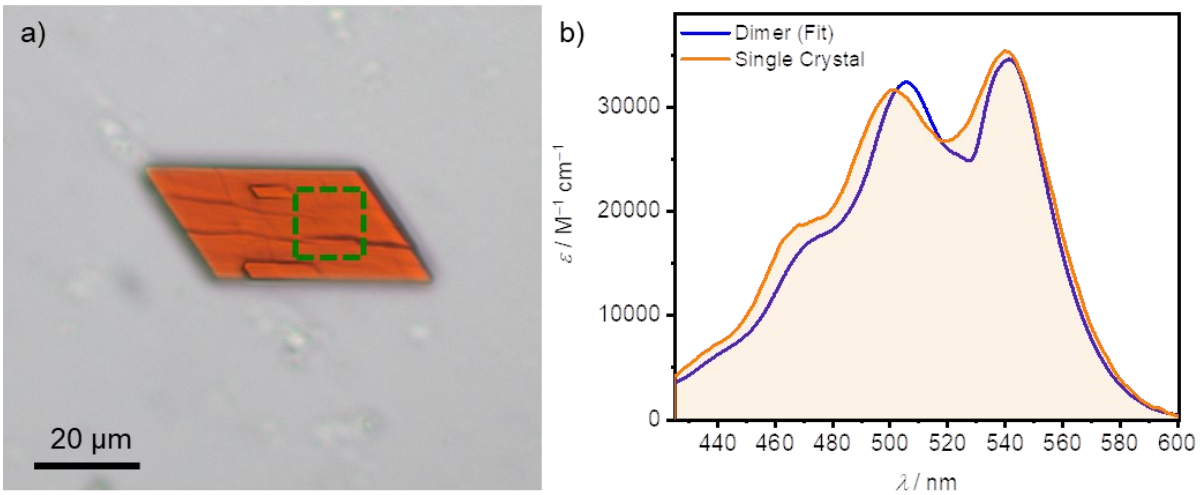

Fig. S30 a) Bright-field optical microscope image of a single crystal of **3a** on a quartz substrate. The green square marks the area where the absorption spectrum was recorded. b) Scaled UV/Vis absorption spectra of a single crystal of PBI **3a** (orange line; see a)) as well as the spectra of a dimer in $CHCl_3$ solution (blue line), as deduced from the global fit analysis of concentration-dependent UV/Vis spectra at 298 K (see Figure S4).

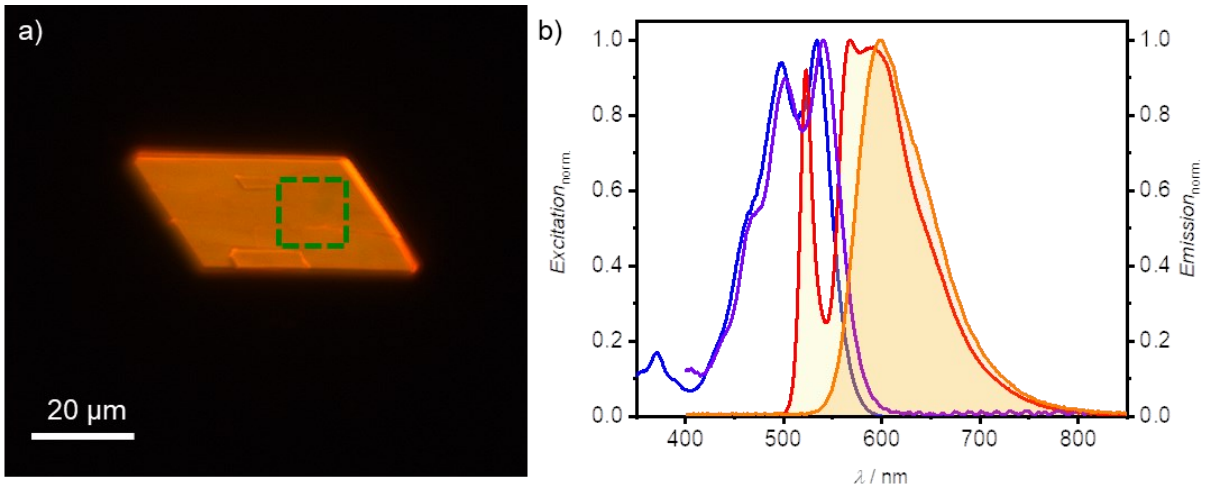

Fig. S31 a) Fluorescence microscope image of a single crystal of **3a** on a quartz substrate upon blue light excitation (464-495 nm). The green square marks the area where the emission spectrum was recorded. b) Normalized excitation (blue, λ_{em} = 700 nm) and emission (red, λ_{ex} = 490 nm) spectra of PBI **3b** in MCH ($c_0 = 1.0 \times 10^{-4}$ M) at 298 K in comparison to the absorption (violet) and emission (orange) spectra of the single crystal of **3a** in (a).

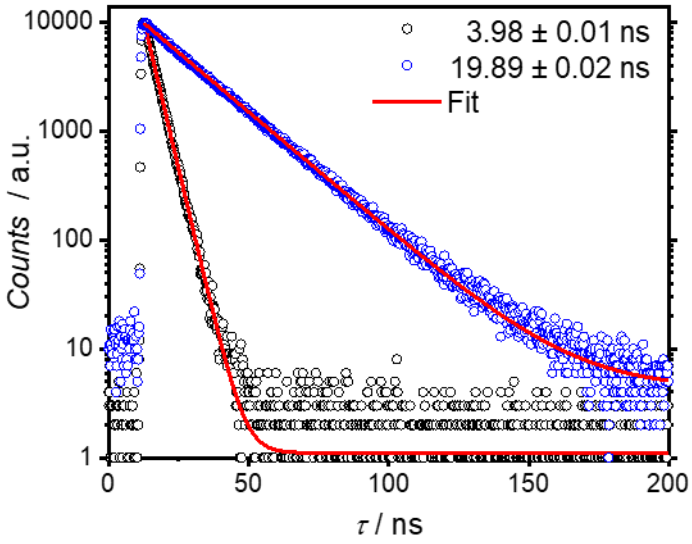

Fig. S32 a) Fluorescence decay curves (symbols) along with their respective fit (red line) of PBI **3b** in MCH solution ($c_0 = 1.0 \times 10^{-4}$ M) at 298 K measured with a front face setup under magic angle conditions (54.7°) after excitation with an EPL laser diode at 505.8 nm and detection at 523 nm (black: Monomer) or 700 nm (blue: Dimer).

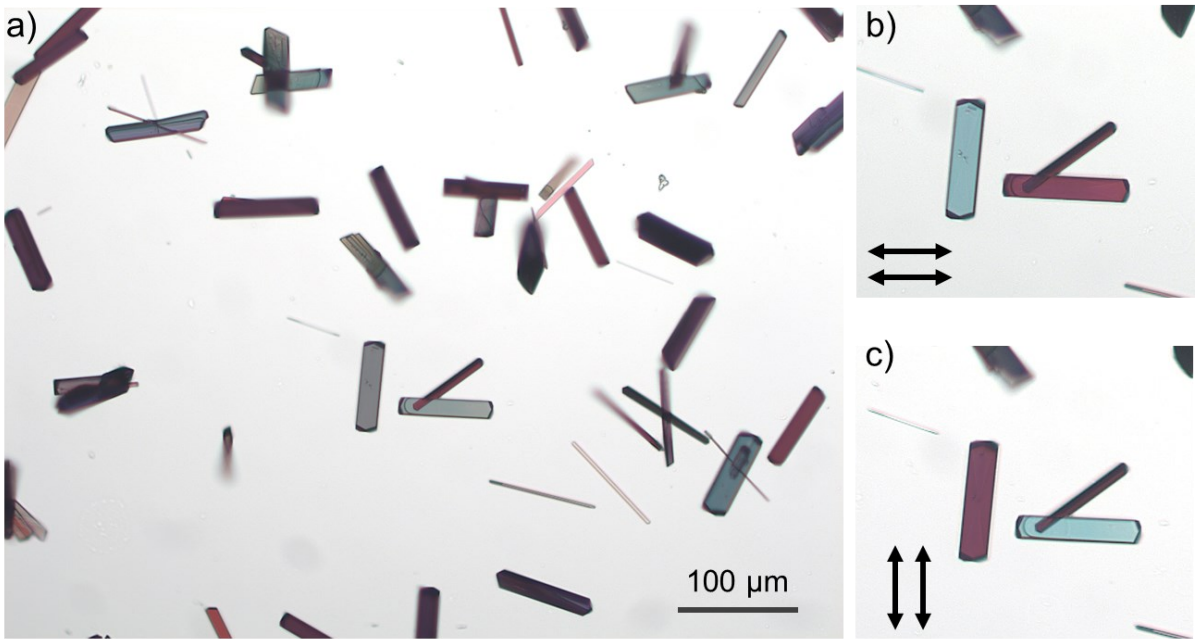

Fig. S33 a) Bright-field optical microscope image of an ensemble of single crystals on a quartz substrate grown from PBI **3a** as host and perylene as guest in 1:2 mixture ($CHCl_3$:MeOH 1:5) a) without as well as b)-c) with parallel aligned polarizer and analyser, both with either b) horizontal or c) vertical orientation.

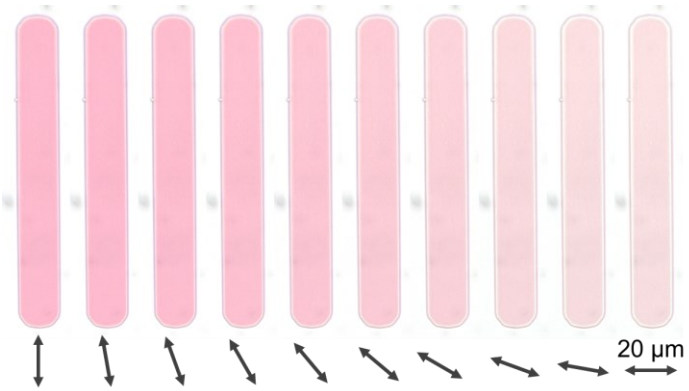

Fig. S34 Polarization-dependent bright-field optical microscope pictures of a thin, red cocrystal of [P·**3a**·P] on a quartz substrate presumable facing up with their (10–1) lattice plane while rotating the polarization axis of the transmitted light in steps of 10° as indicated by the arrow.

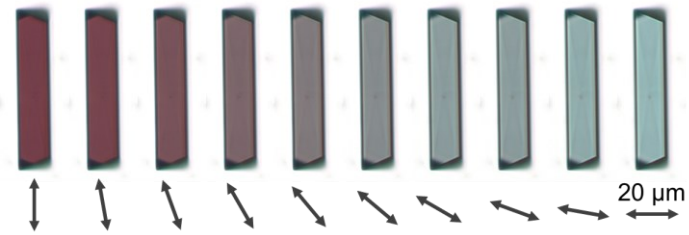

Fig. S35 Polarization-dependent bright-field optical microscope pictures of a thick, violet cocrystal of [P·**3a**·P] on a quartz substrate presumable facing up with their (101) lattice plane while rotating the polarization axis of the transmitted light in steps of 10° as indicated by the arrow.

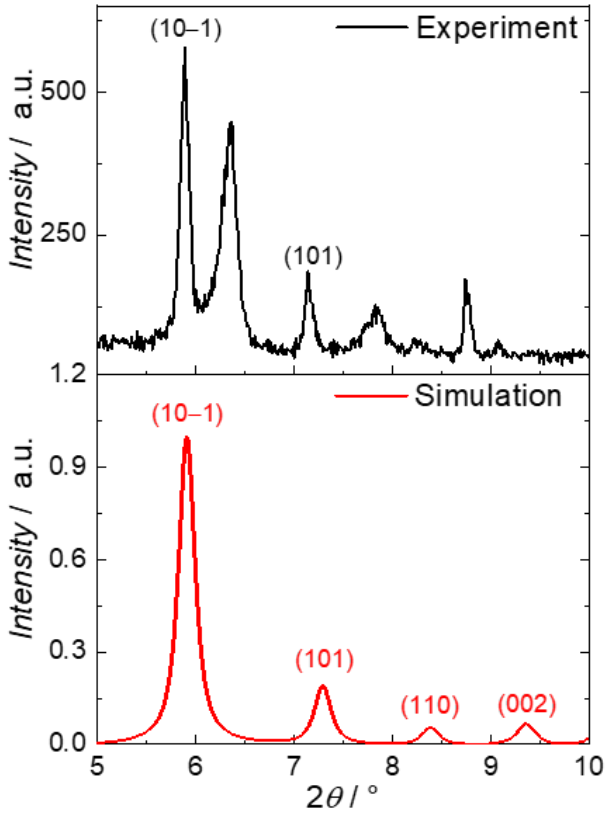

Fig. S36 XRD pattern (black, top) of an ensemble of single crystals on a quartz substrate grown from PBI **3a** as host and perylene as guest in 1:2 mixture ($CHCl_3$:MeOH 1:5) in comparison with a powder pattern (red, bottom) simulated from the single-crystal structure as well as indexed reflexes arising from different sets of lattice planes.

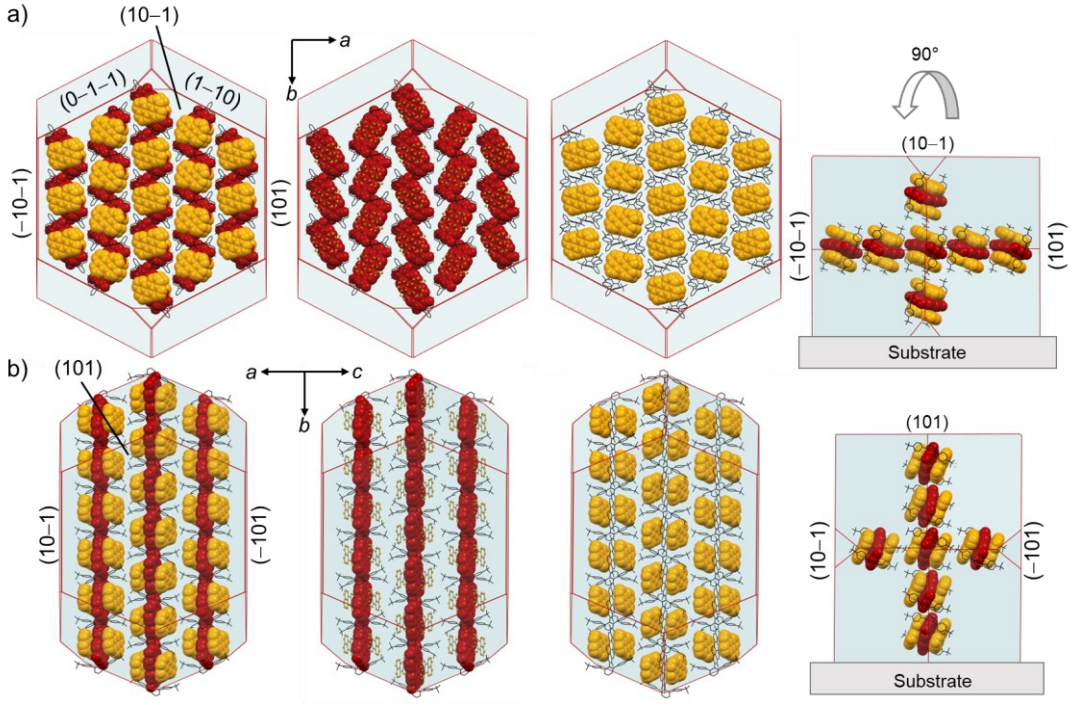

Fig. S37 BFDH morphology of the single crystal of cocrystal [P·**3a**·P] as viewed onto the a) (10–1) or b) (101) planes with indexed relevant lattice planes (left), highlighting once the PBI host (red) or perylene guest (orange) molecules (middle), as well as visualization of relative orientation on the substrate (right, each after 90° rotation).

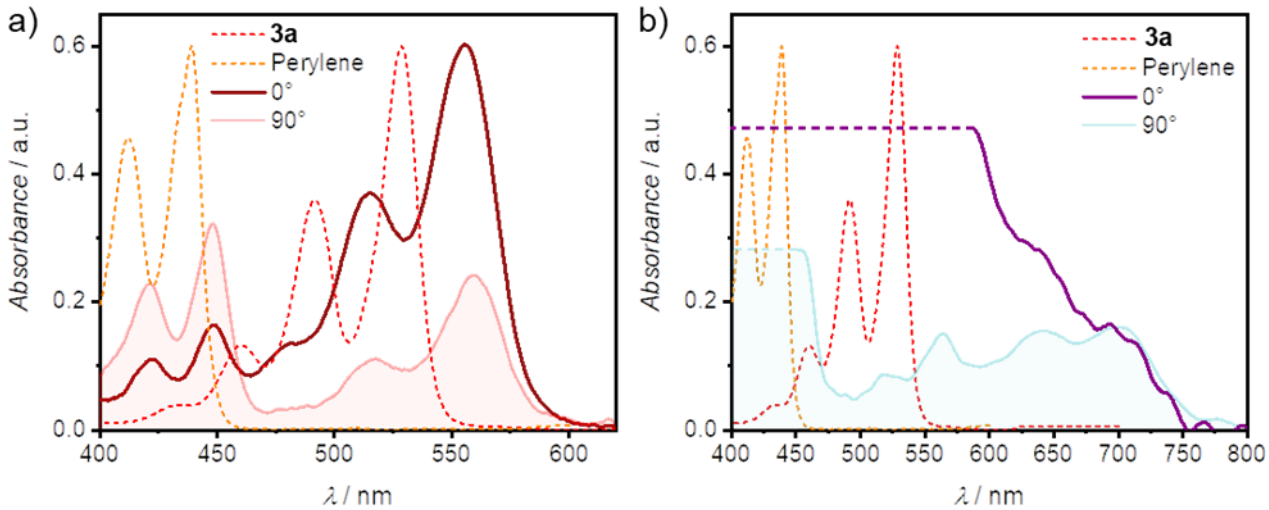

Fig. S38 Polarization-dependent (0° & 90°) UV/Vis absorption spectra of cocrystals [P·**3a**·P] on a quartz substrate presumable facing up with their a) (10–1) (dark and light red) or b) (101) (violet and turquoise) lattice planes (see Figs. S21-23) as well as the scaled spectra of PBI **3a** (red dashed line) and perylene (orange dashed line) in $CHCl_3$ at 298 K.

9. Theoretical calculations (complexes)

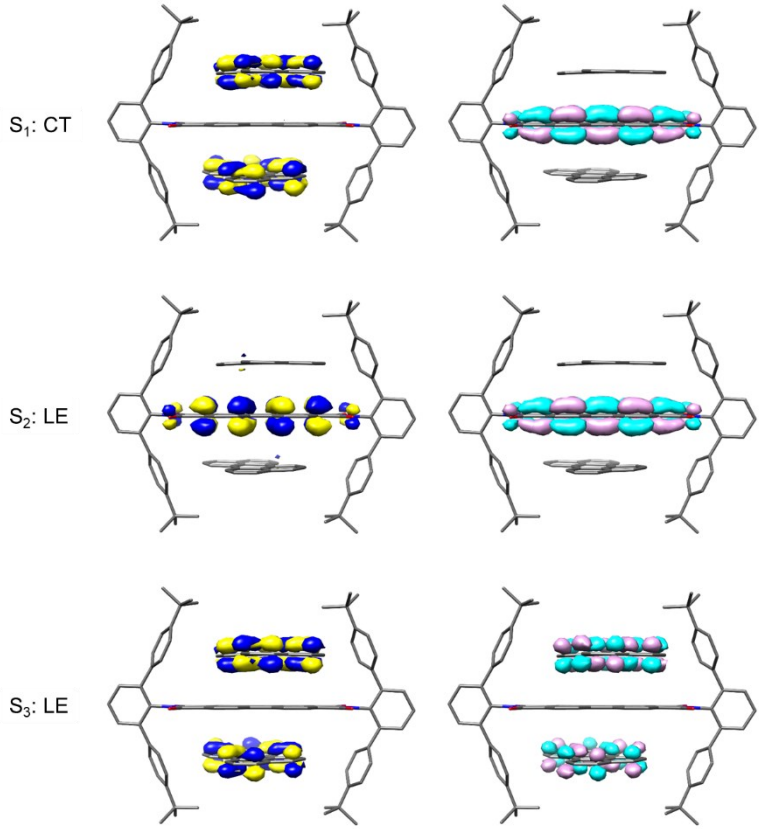

Fig. S39 Optimized geometry and occupied (left) as well as virtual (right) NTOs of complex [P·**3a**·P].

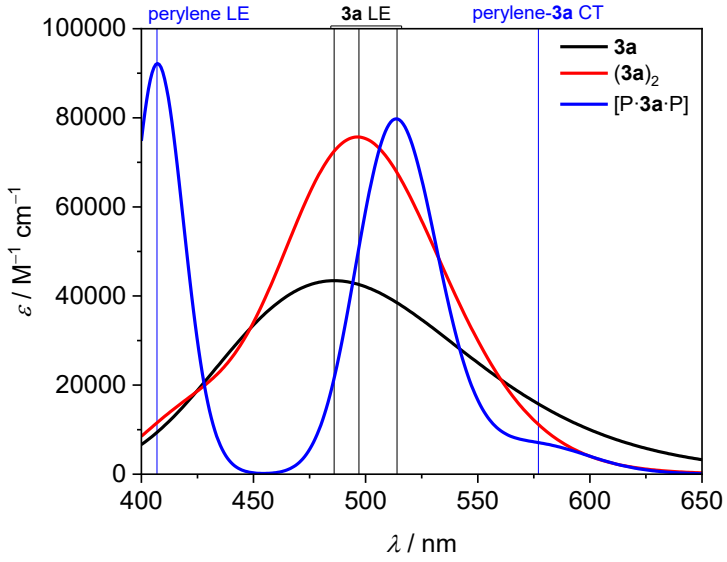

Fig. S40 Calculated unmodified UV/Vis absorption spectra of **3a**, its dimer (**3a**)$_2$ and the host-guest complex [P·**3a**·P].

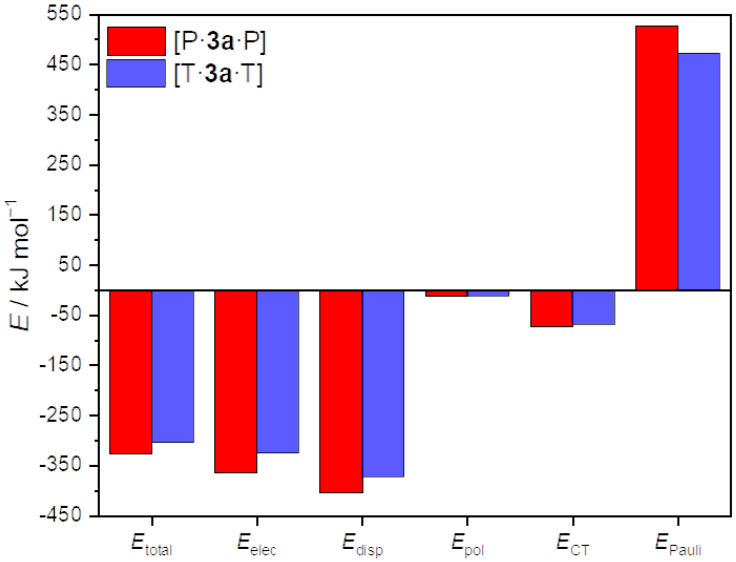

Fig. S41 ALMO-EDA values computed for [P·**3a**·P] and [T·**3a**·T]. Components of the total energy (E_{total}): E_{elec}: electrostatic; E_{disp}: dispersion; E_{pol}: polarization; E_{CT}: charge-transfer; E_{Pauli}: Pauli-repulsion. E_{total}: is the sum of these components.

10. NMR spectra

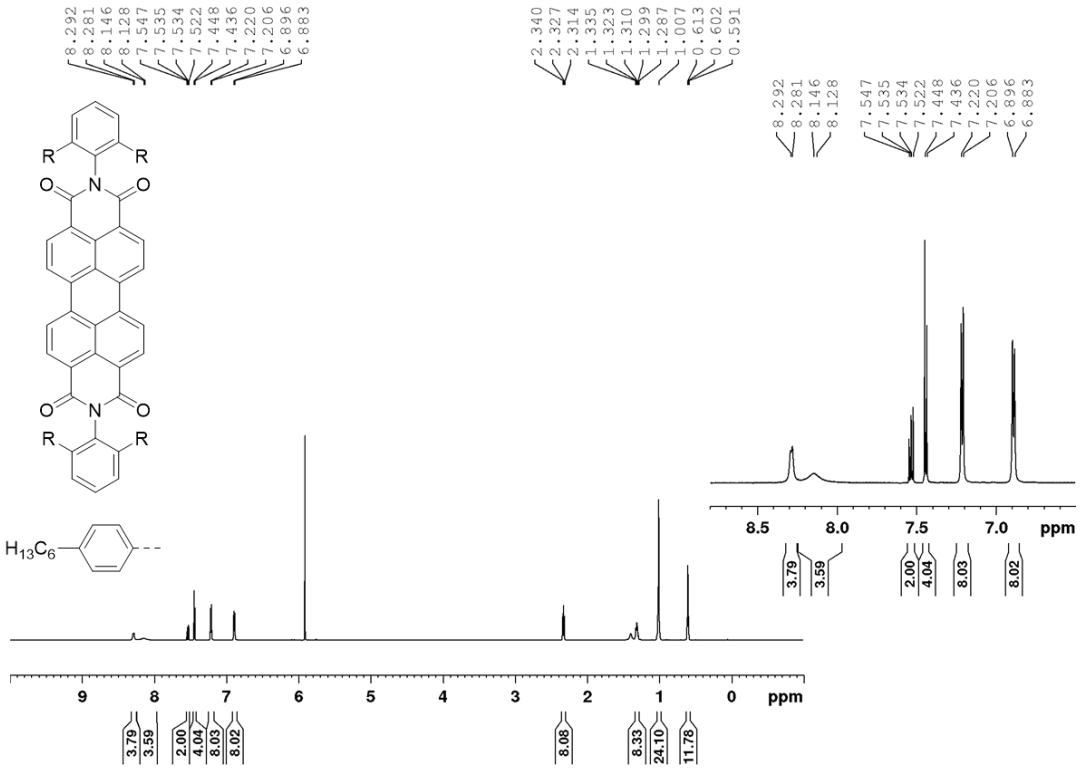

Fig. S42 ^{1}H NMR spectrum (600 MHz) of **3b** in $C_2D_2Cl_4$ at 368 K.

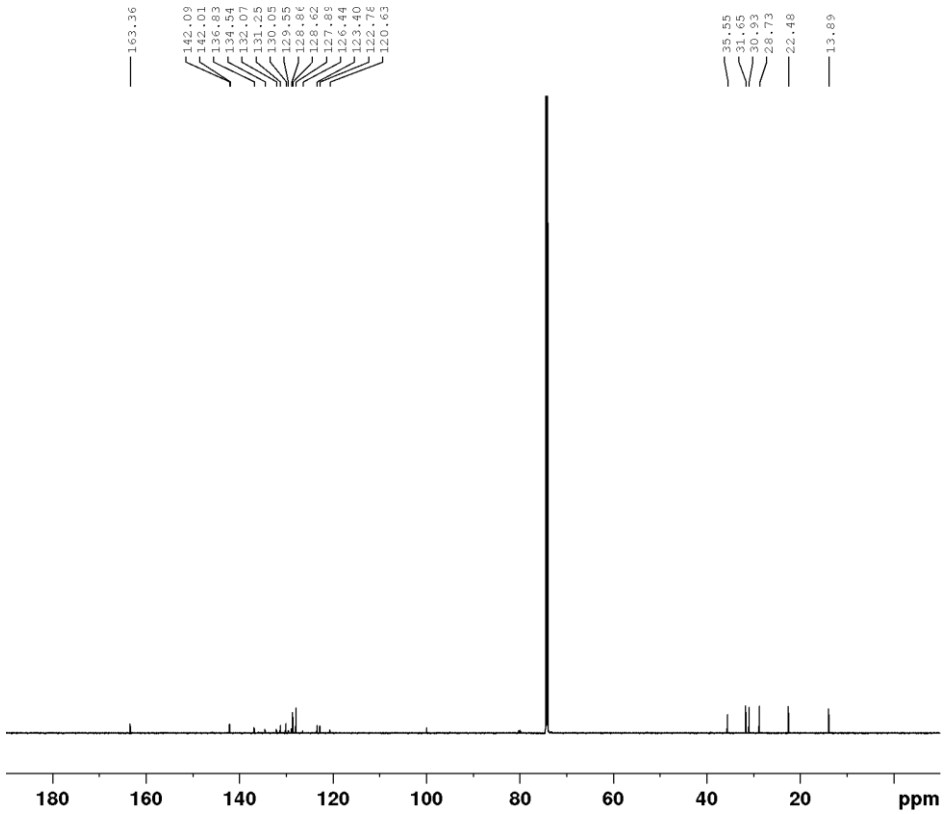

Fig. S43 ^{13}C NMR spectrum (151 MHz) of **3b** in $C_2D_2Cl_4$ at 368 K.

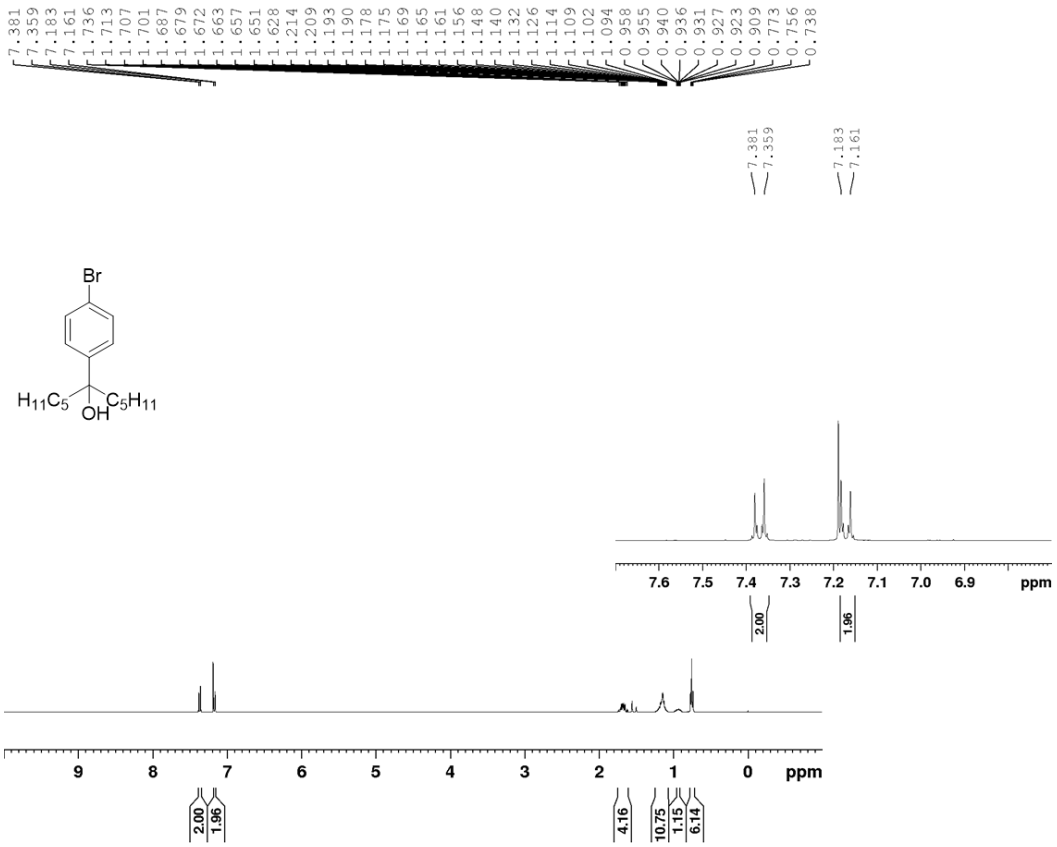

Fig. S44 ^{1}H NMR spectrum (400 MHz) of **10** in $CDCl_3$ at 298 K.

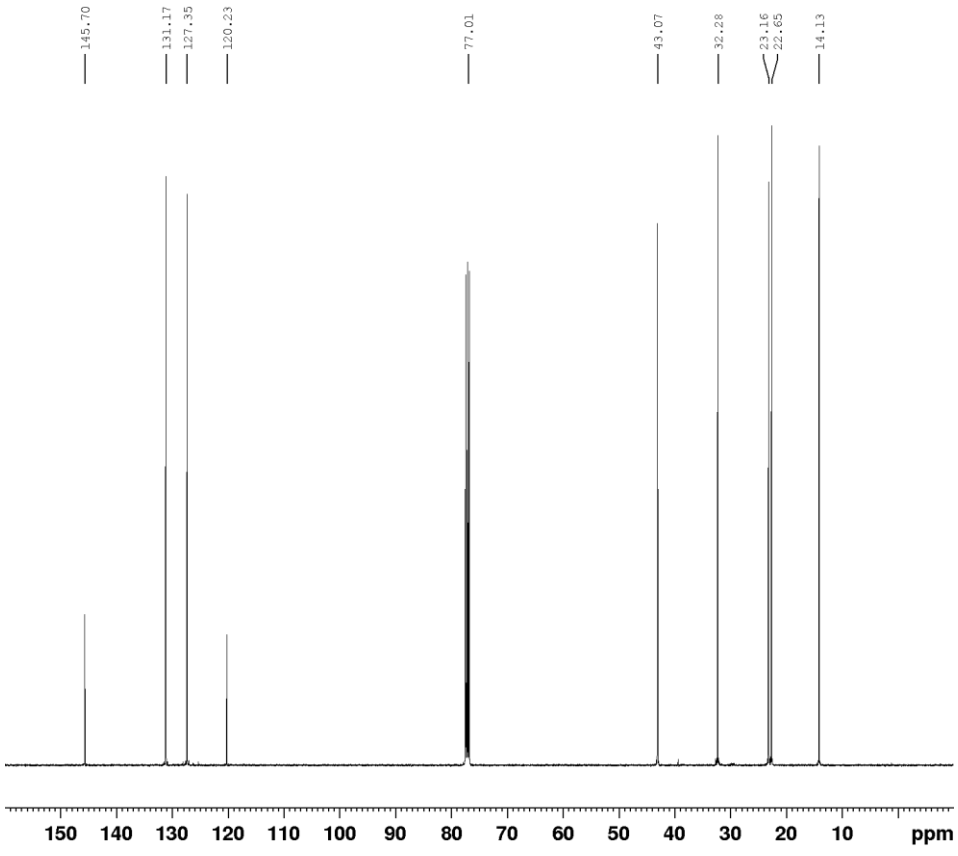

Fig. S45 ^{13}C NMR spectrum (101 MHz) of **10** in $CDCl_3$ at 298 K.

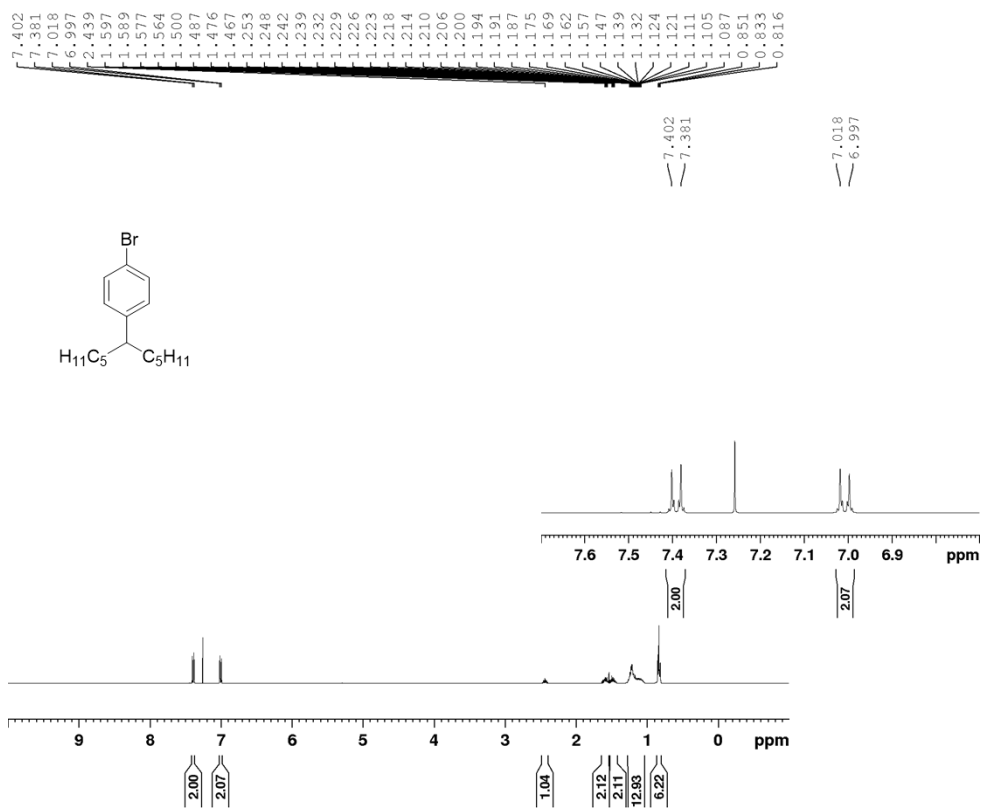

Fig. S46 ^{1}H NMR spectrum (400 MHz) of **4c** in $CDCl_3$ at 298 K.

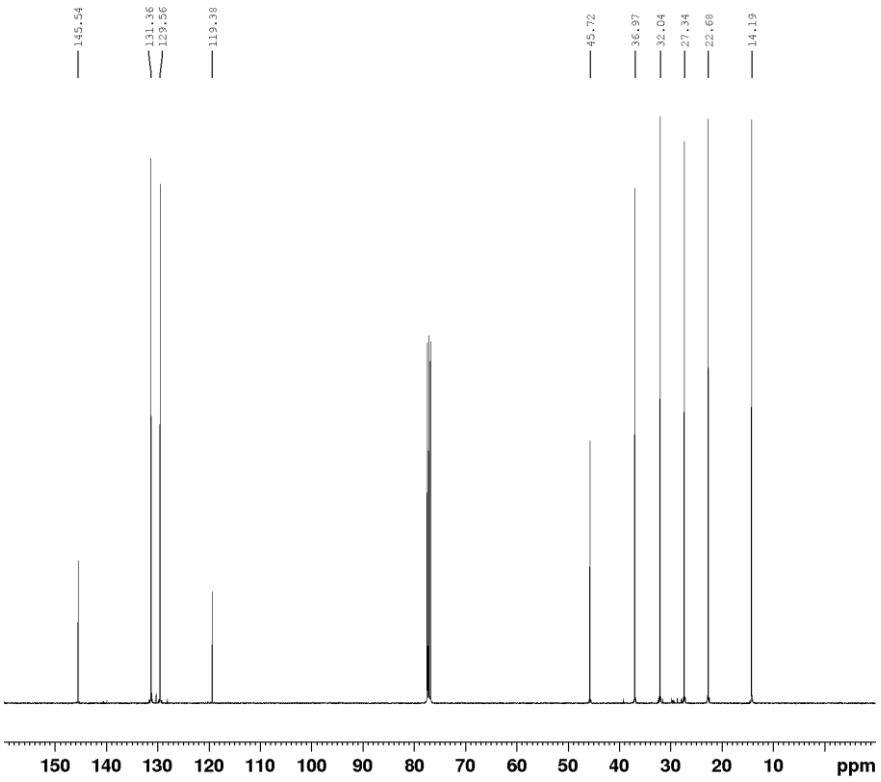

Fig. S47 ^{13}C NMR spectrum (101 MHz) of **4c** in $CDCl_3$ at 298 K.

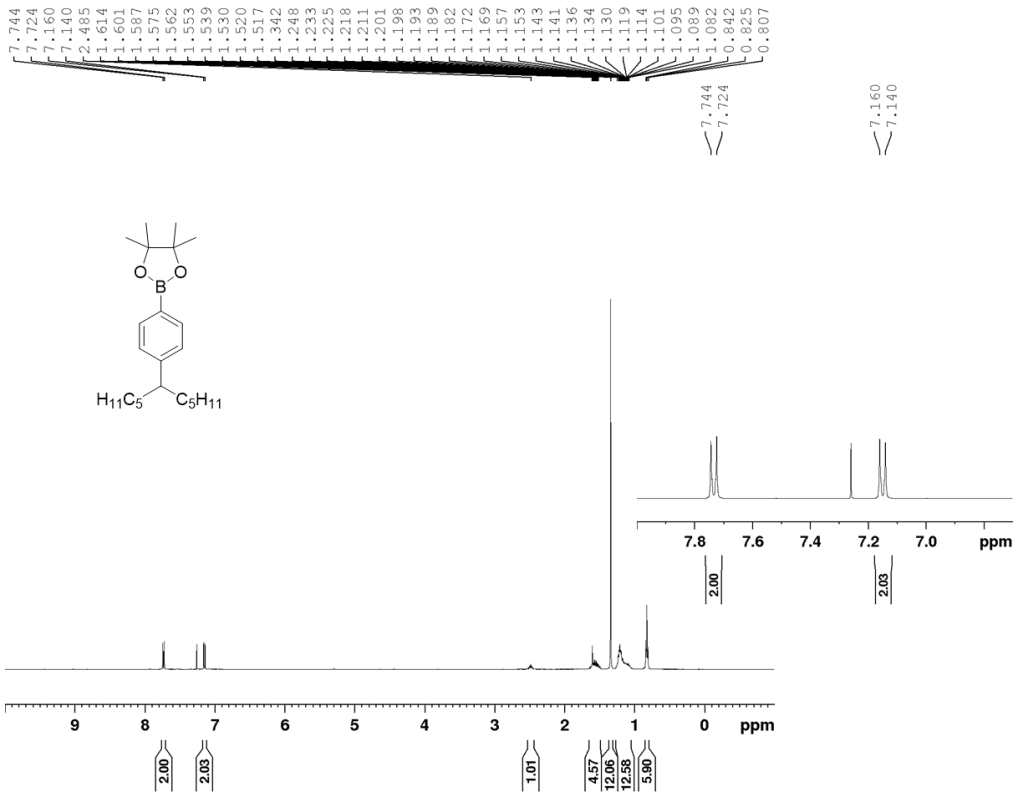

Fig. S48 ^{1}H NMR spectrum (400 MHz) of **6c** in $CDCl_3$ at 298 K.

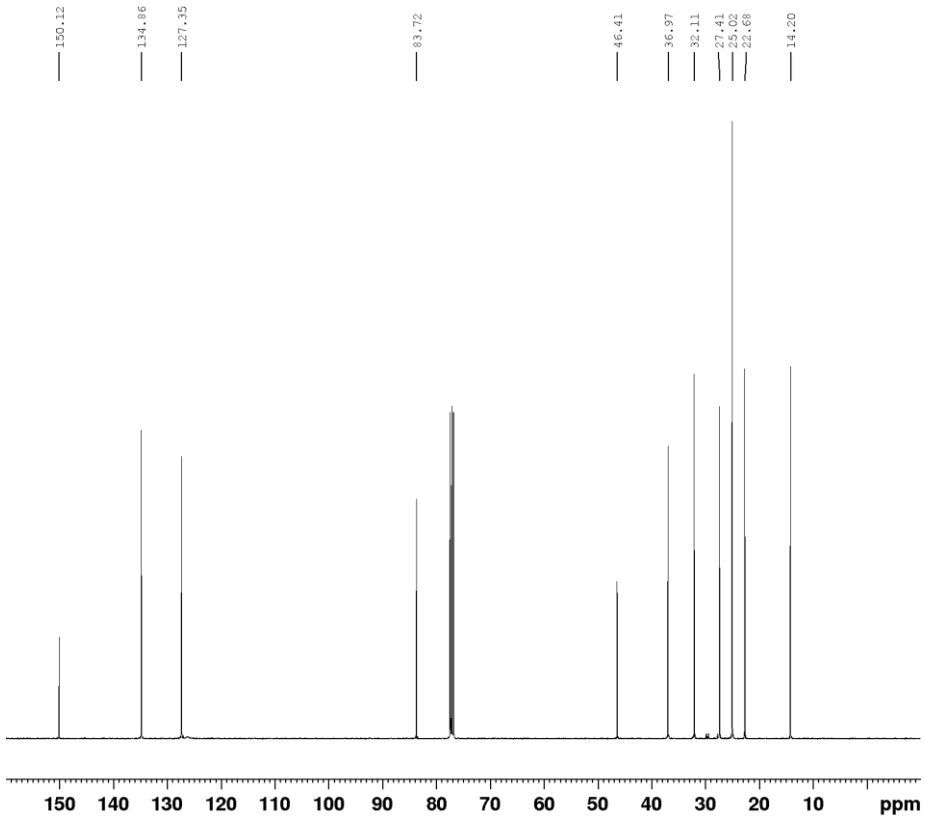

Fig. S49 ^{13}C NMR spectrum (101 MHz) of **6c** in $CDCl_3$ at 298 K.

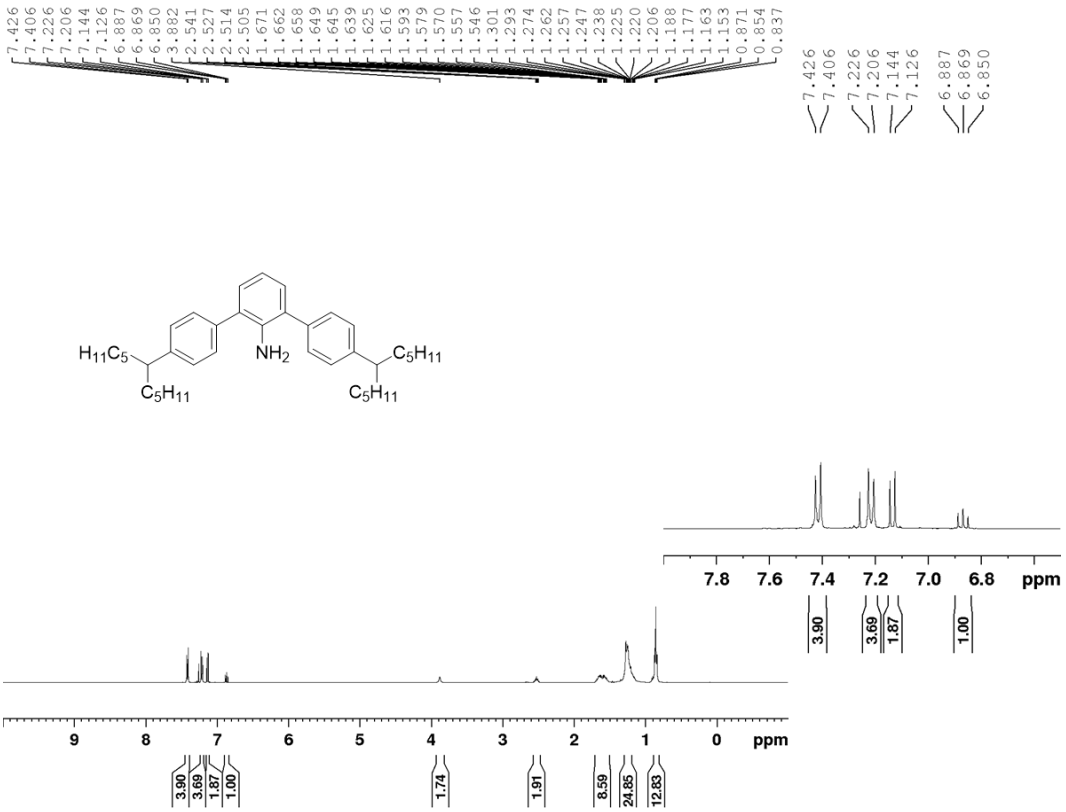

Fig. S50 ^{1}H NMR spectrum (400 MHz) of **2c** in $CDCl_3$ at 298 K.

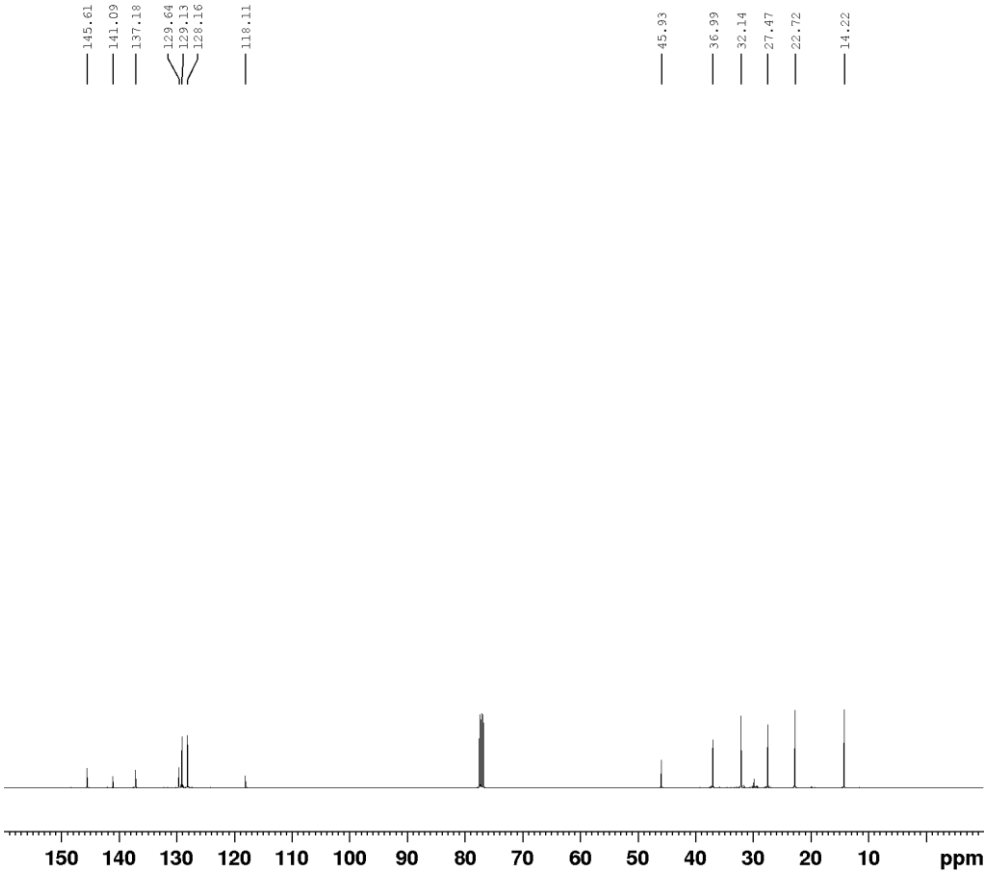

Fig. S51 ^{13}C NMR spectrum (101 MHz) of **2c** in $CDCl_3$ at 298 K.

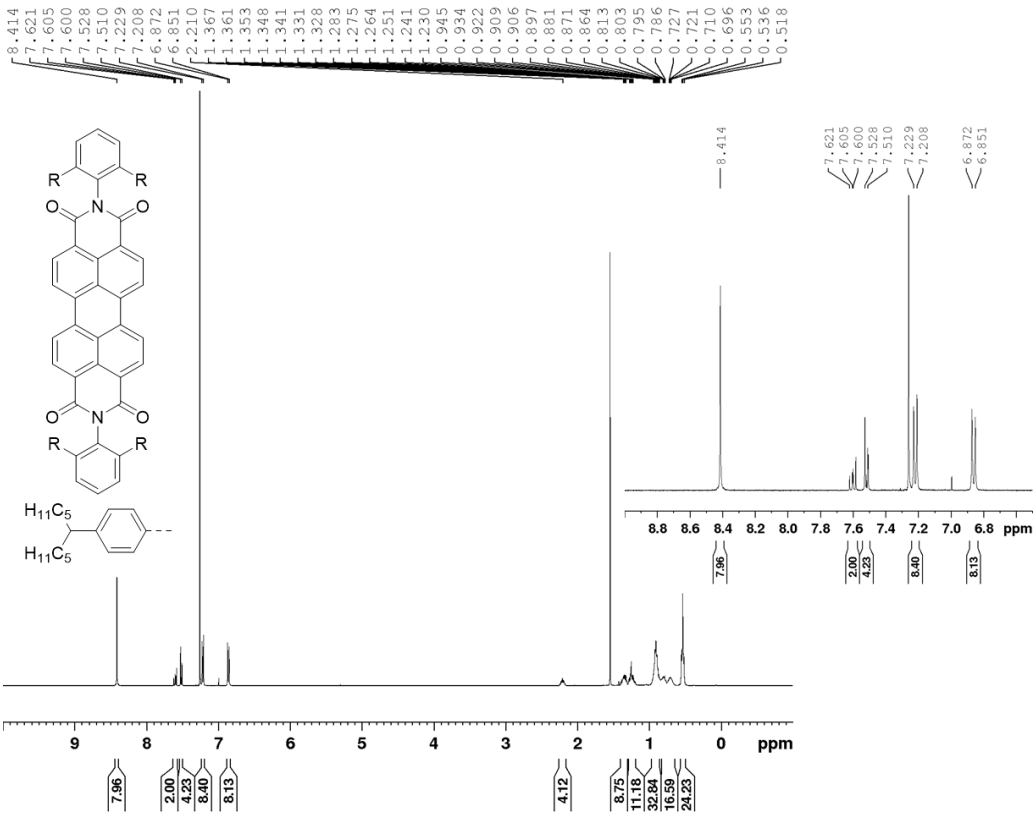

Fig. S52 ^{1}H NMR spectrum (600 MHz) of **3c** in $CDCl_3$ at 298 K.

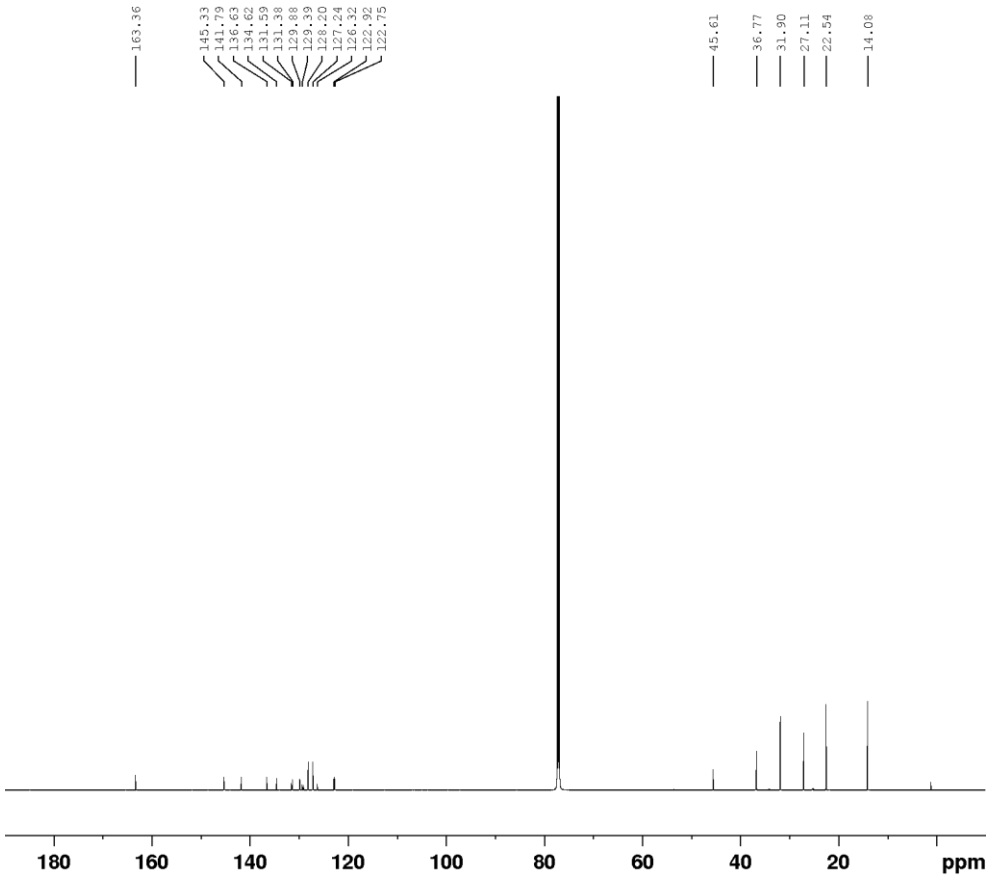

Fig. S53 ^{13}C NMR spectrum (151 MHz) of **3c** in $CDCl_3$ at 298 K.

11. Mass spectrometry

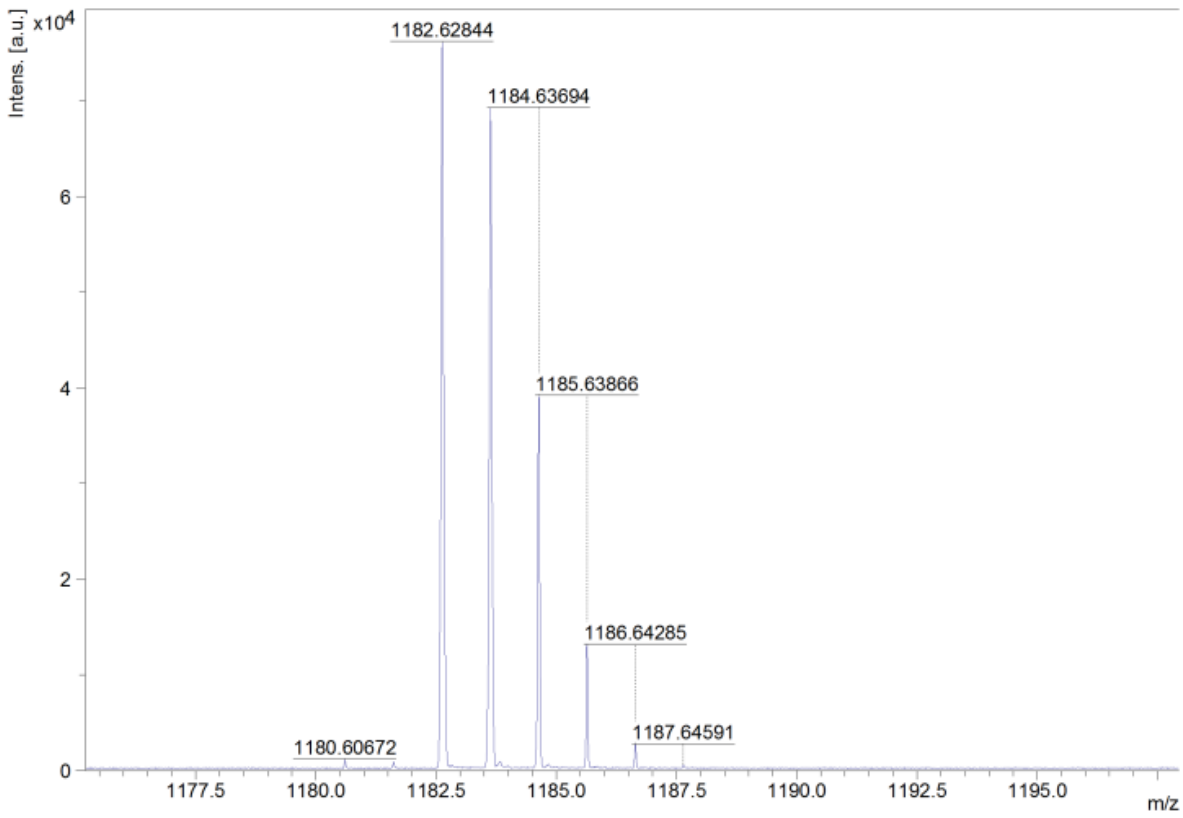

Fig. S54 High-resolution mass spectrum (MALDI-TOF, neg. mode, matrix: DCTB 1:3 in chloroform) of **3b**.

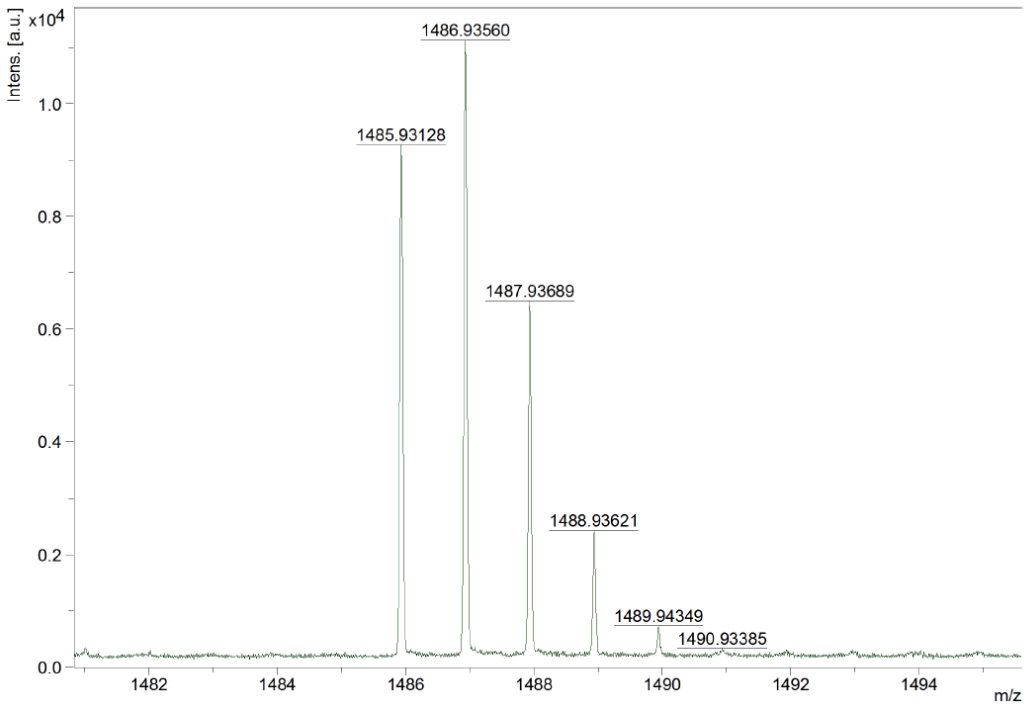

Fig. S55 High-resolution mass spectrum (MALDI-TOF, pos. mode, matrix: DCTB 1:3 in chloroform) of **3c**.

12. References

S1 M. Mahl, K. Shoyama, A.M. Krause, D. Schmidt and F. Würthner, *Angew. Chem. Int. Ed.*, 2020, **59**, 13401-13405.

S2 D. Meinhard, M. Wegner, G. Kipiani, A. Hearley, P. Reuter, S. Fischer, O. Marti and B. Rieger, *J. Am. Chem. Soc.*, 2007, **129**(29), 9182-9191.

S3 K. Menekse, M. Mahl, J. Albert, M. A. Niyas, K. Shoyama, M. Stolte and F. Würthner, *Sol. RRL.*, 2023, **7**, 2200895.

S4 M. Banerjee, R. Shukla and R. Rathore, *J. Am. Chem. Soc*., 2009, **131**, 1780-1786.

S5 D. Wang, M. R. Talipov, M. V. Ivanov and R. Rathore, *J. Am. Chem. Soc.*, 2016, **138**, 16337-16344.

S6 K. Shoyama, M. Mahl, S. Seifert and F. Würthner, *J. Org. Chem.*, 2018, **83**, 5339-5346.

S7 bindfit (Supramolecular, 2020); http://supramolecular.org.

S8 P. Thordarson, *Chem. Soc. Rev.*, 2011, **40**, 1305-1323.

S9 G. M. Sheldrick, *Acta Crystallogr. A*, 2015, **71**, 3-8.

S10 G. M. Sheldrick, *Acta Crystallogr. A*, 2008, **64**, 112-122.

S11 A. L. Spek, *Acta Crystallogr. C*, 2015, **71**, 9-18.

S12 A. L. Spek, *Acta Crystallogr. D*, 2009, **71**, 148-155.

S13 (a) C. Bannwarth, E. Caldeweyher, S. Ehlert, A. Hansen, P. Pracht, J. Seibert, S. Spicher and S. Grimme, *WIREs Comput*. *Mol*. *Sci*., 2020, **11**, e01493; (b) C. Plett and S. Grimme, *Angew. Chem. Int. Ed.*, 2023, **62**, e202214477.

S14 C. Bannwarth, S. Ehlert and S. Grimme, *J*. *Chem*. *Theory Comput*., 2019, **15**, 1652.

S15 F. Neese, F. Wennmohs, U. Becker and C. Riplinger, *J. Chem. Phys.*, 2020, **152**, 224108.

S16 S. Grimme, A. Hansen, S. Ehlert and J.-M. Mewes, *J*. *Chem*. *Phys*., 2021, **154**, 064103.

S17 C. Kaufmann, D. Bialas, M. Stolte and F. Würthner, *J. Am. Chem. Soc.*, 2018, **140**, 9986.

S18 M. E. Madjet, A. Abdurahman, and T. Renger, *J*. *Phys*. *Chem*. *B*, 2006, **110**, 17268.

S19 T. Lu and F. Chen, *J*. *Comput*. *Chem*., 2012, **33**, 580.

S20 M. J. Frisch, G. W. Trucks, H. B. Schlegel, G. E. Scuseria, M. A. Robb, J. R. Cheeseman, G. Scalmani, V. Barone, G. A. Petersson, H. Nakatsuji, X. Li, M. Caricato, A. V. Marenich, J. Bloino, B. G. Janesko, R. Gomperts, B. Mennucci, H. P. Hratchian, J. V. Ortiz, A. F. Izmaylov, J. L. Sonnenberg, D. Williams-Young, F. Ding, F. Lipparini, F. Egidi, J. Goings, B. Peng, A. Petrone, T. Henderson, D. Ranasinghe, V. G. Zakrzewski, J. Gao, N. Rega, G. Zheng, W. Liang, M. Hada, M. Ehara, K. Toyota, R. Fukuda, J. Hasegawa, M. Ishida, T. Nakajima, Y. Honda, O. Kitao, H. Nakai, T. Vreven, K. Throssell, J. A. Montgomery, Jr., J. E. Peralta, F. Ogliaro, M. J. Bearpark, J. J. Heyd, E. N. Brothers, K. N. Kudin, V. N. Staroverov, T. A. Keith, R. Kobayashi, J. Normand, K. Raghavachari, A. P. Rendell, J. C. Burant, S. S. Iyengar, J. Tomasi, M. Cossi, J. M. Millam, M. Klene, C. Adamo, R. Cammi, J. W. Ochterski, R. L. Martin, K. Morokuma, O. Farkas, J. B. Foresman and D. J. Fox, *Gaussian, Inc., Wallingford CT*, 2016.

S21 (a) G. te Velde, F. M. Bickelhaupt, E. J. Baerends, C. Fonseca Guerra, S. J. A. van Gisbergen, J. G. Snijders and T. Ziegler, *J. Comput. Chem.*, 2001, **22**, 931; (b) C. Fonseca Guerra, J. G. Snijders, G. te Velde and E. J. Baerends, *Theor. Chem. Acc.*, 1998, **99**, 391; (c) ADF2013, SCM, Theoretical Chemistry; Vrije Universiteit: Amsterdam, The Netherlands; http://www.scm.com

S22 P. R. Horn, Y. Mao, and M. Head-Gordon, *Phys*. *Chem*. *Chem*. *Phys*., 2016, **18**, 23067.

S23 Y. Shao et al., *Mol. Phys*., 2015, **113**, 184.

S24 E. F. Pettersen, T. D. Goddard, C. C. Huang, G. S. Couch, D. M. Greenblatt, E. C. Meng and T. E. Ferrin, *J. Comput. Chem.*, 2004, **25**, 1605-1612.

S24 N. J. Hestand and F. Spano, *Acc. Chem. Res.*, 2017, **50**, 341.

S25 X. Zhang, X. Jiang, K. Zhang, L. Mao, J. Luo, C. Chi, H. S. O. Chan and J. Wu, *J. Org. Chem*., 2010, **75**, 8069-8077.

S26 F. Neese, F. Wennmohs, U. Becker and C. Riplinger, *J. Chem. Phys.*, 2020, **152**, 224108.

S27 Vander Griend DA. SIVVU http://sivvu.org/ (accessed July 27th, 2023).